

Optical and Infrared Photometry of the Unusual Type Ia Supernova 2000cx

P. Candia, K. Krisciunas, Nicholas B. Suntzeff, D. González, J. Espinoza, R. Leiton, A.
Rest, and R. C. Smith

*Cerro Tololo Inter-American Observatory, National Optical Astronomy Observatories,¹
Casilla 603, La Serena, Chile*
pcandia@ctio.noao.edu, kkrisciunas@noao.edu, nsuntzeff@noao.edu, leiton@ctio.noao.edu,
arest@noao.edu, csmith@noao.edu

J. Cuadra

Pontificia Universidad Católica de Chile, Santiago, Chile
jcuada@puc.cl

T. Tavenner

*New Mexico State University, Astronomy Department, Box 30001, MSC 4500, Las Cruces,
NM 88003-8001*
tanya@nmsu.edu

C. Logan

*Department of Earth, Atmospheric, and Planetary Sciences, Massachusetts Institute of
Technology, Cambridge, MA 02139*
clogan@mit.edu

K. Snider, M. Thomas, and A. A. West

Department of Astronomy, University of Washington, Box 351580, Seattle, WA 98195
ksnider@u.washington.edu, drtas@u.washington.edu, west@astro.washington.edu

G. González

Iowa State University, Department of Physics and Astronomy, Ames, IA 50011-3160
gonzog@iastate.edu

S. González and M. M. Phillips

Las Campanas Observatory, Casilla 601, La Serena, Chile
sergiogonzalezctio@yahoo.com, mmp@lco.cl

N. C. Hastings and R. McMillan

*Apache Point Observatory, Astrophysical Research Consortium, 2001 Apache Point Road,
P. O. Box 59, Sunspot, NM 88349-0059
hastings@apo.nmsu.edu, mcmillan@apo.nmsu.edu*

ABSTRACT

We present optical and infrared photometry of the unusual Type Ia supernova 2000cx. With the data of Li et al. (2001) and Jha (2002), this comprises the largest dataset ever assembled for a Type Ia SN, more than 600 points in *UBVRIJHK*. We confirm the finding of Li et al. regarding the unusually blue $B - V$ colors as SN 2000cx entered the nebular phase. Its *I*-band secondary hump was extremely weak given its *B*-band decline rate. The V minus near infrared colors likewise do not match loci based on other slowly declining Type Ia SNe, though $V - K$ is the least “abnormal”. In several ways SN 2000cx resembles other slow decliners, given its *B*-band *decline* rate ($\Delta m_{15}(B) = 0.93$), the appearance of Fe III lines and weakness of Si II in its pre-maximum spectrum, the $V - K$ colors and post-maximum $V - H$ colors. If the distance modulus derived from Surface Brightness Fluctuations of the host galaxy is correct, we find that the rate of light increase prior to maximum, the characteristics of the bolometric light curve, and the implied absolute magnitude at maximum are all consistent with a sub-luminous object with $\Delta m_{15}(B) \approx 1.6$ -1.7 having a higher than normal kinetic energy.

Keywords: (stars:) supernovae: individual, SN 2000cx, SN 1986G, SN 1999aa, SN 1999ac, SN 1999aw, SN 1999ee, SN 1999gp, SN 2000bk, SN 2001ba, SN 2001el; infrared: stars; techniques: photometric

1. Introduction

Astronomers try to understand the universe by looking for patterns in observed phenomena. Often, the patterns themselves are reason to believe in underlying, understandable physical mechanisms, while at other times the exceptions to the rules provide the motivation to expand our conceptions of the physical makeup of cosmic objects. In this paper we

¹The National Optical Astronomy Observatories are operated by the Association of Universities for Research in Astronomy, Inc., under cooperative agreement with the National Science Foundation.

present optical and infrared photometry of the very unusual supernova 2000cx. Previous optical data have been presented by Li et al. (2001), who describe SN 2000cx as “unique”.

SN 2000cx was discovered by Yu, Modjaz, & Li (2000) from images taken on 17.5 and 18.4 July 2000 UT as part of the Lick Observatory Supernova Search, using the 0.76-m Katzman Automatic Imaging Telescope (KAIT). This object was located at $\alpha = 1:24:46.15$, $\delta = +9^\circ 30' 30''.9$ (equinox 2000.0), which is $23''.0$ west and $109''.3$ south of the nucleus of the S0 galaxy NGC 524. A spectrum taken on 23 July UT with the Nickel 1-m reflector at Lick Observatory (Chornock et al. 2000) revealed that the object was a peculiar Type Ia supernova, resembling SN 1991T a few days before maximum brightness, with prominent Fe III absorption lines near 430 and 490 nm but weak Si II at 612 nm. Optical photometry (Li et al. 2001) revealed that SN 2000cx is different from all known Type Ia SNe and that the light curves cannot be fitted well using the techniques currently available. The pre-maximum rise was relatively fast, similar to SN 1994D, but the post-maximum decline was relatively slow, similar to SN 1991T.

We present optical and infrared photometry of SN 2000cx, initiated at CTIO with the Yale-AURA-Lisbon-Ohio (YALO) 1-m telescope on 19 July 2000 (UT), some 8 days before the time of *B*-band maximum. We include data taken with the 0.76-m Manastash Ridge Observatory (MRO) of the University of Washington (also begun on 19 July UT), the CTIO 0.9-m telescope, and the Apache Point Observatory 3.5-m telescope (APO). The calibration of the infrared light curves was primarily made possible with observations made with the Swope 1-m telescope at Las Campanas Observatory.

2. Observations

The YALO optical images were obtained using a Loral 2048×2048 CCD with a scale of $0''.30$ per pixel, giving roughly a $10' \times 10'$ field of view. Due to amplifier problems only half of the chip was working before September 2000. On 6 September 2000 this problem was fixed, but it was necessary to change the gain from 6.6 to 3.6 electrons per ADU. The readnoise improved from 14.2 to 11 electrons. The broadband *JHK* images from the YALO telescope were obtained using a 1024×1024 HgCdTe HAWAII Array from Rockwell. The filters have over an 80 percent transmittance from 1.171 to $1.322 \mu\text{m}$ for the *J*-band, 1.498 to $1.766 \mu\text{m}$ for *H* and 2.012 to $2.278 \mu\text{m}$ for *K*. The scale of the infrared CCD is $0''.20$ per pixel, making a total field of view of $3'.3 \times 3'.3$.

The camera used at the CTIO 0.9-m telescope contains the #3 Tektronix 2048 CCD, which is a thinned, anti-reflection coated, back-side illuminated chip with $2\text{K} \times 2\text{K}$ pixels.

The scale and field size are $0''.40$ per pixel and $13'.5$, respectively. The filters used were: U (liquid CuSO_4), $\lambda_0 = 3575 \text{ \AA}$, $\text{FWHM} = 600 \text{ \AA}$; B , $\lambda_0 = 4202 \text{ \AA}$, $\text{FWHM} = 1050 \text{ \AA}$; V , $\lambda_0 = 5475 \text{ \AA}$, $\text{FWHM} = 1000 \text{ \AA}$; R , $\lambda_0 = 6425 \text{ \AA}$, $\text{FWHM} = 1500 \text{ \AA}$; I_{KC} , $\lambda_0 = 8075 \text{ \AA}$, $\text{FWHM} = 1500 \text{ \AA}$. The $UBVRI_{KC}$ filters were from the CTIO facility set Tek #1.

Traces of the filters used with the YALO and CTIO 0.9-m telescopes are shown in Stritzinger et al. (2002). However, for our SN 2000cx observations with YALO we did *not* use the very broad, non-standard R filter used by Stritzinger et al. Instead, we used a much narrower, more standard filter (see Appendix).

The APO 3.5-m optical images were obtained using the facility CCD imager SPIcam, which contains a back-side illuminated SITe chip of 2048×2048 pixels. 2×2 readout was used, giving a scale of $0''.28$ per pixel and a $4'.78 \times 4'.78$ field of view. The APO infrared images were obtained with the 3.5-m telescope using GRIM II, which contains a Rockwell 256×256 NICMOS3 HgCdTe array. The chip is sensitive from 1 to $2.5 \mu\text{m}$ with a quantum efficiency of approximately 70 percent, a gain of 4.7 electrons per ADU, and a readnoise of 110 electrons. The J , H and K' filters transmit at 1.265 ± 0.267 , 1.646 ± 0.339 , and $2.114 \pm 0.343 \mu\text{m}$, respectively.

The CCD camera at the MRO 0.76-m telescope uses a Ford Aerospace chip of 1024×1024 pixels, with a readnoise of 8 electrons. The scale is $0''.61$ per pixel, giving a $10'.32 \times 10'.32$ field of view. It contains $UBVRI$ “Harris” filters.

Instrumental YALO and 0.9-m magnitudes were measured as Point Spread Function (PSF) magnitudes using the DAOPHOT package (Stetson 1987, 1990). A transformation equation of the form $m = f(\text{M,I,X,T})$, as suggested by Harris, Fitzgerald, & Reed (1981), was used. Here m is the observed (i.e. instrumental) magnitude, M is the tabulated magnitude (e.g. from Landolt 1992), I is the tabulated color index, X is the airmass, and T is the time during the night.

Using the observations of the Landolt (1992) standards, we determined zeropoints, color terms and atmospheric terms. This allowed us to calibrate the field stars near SN 2000cx. Photometry of the supernova itself is then tied to the Landolt standards via these field stars. This allows us to derive accurate values for the SN even if it is observed under non-photometric conditions. Once the field star sequences were established, we dropped the airmass term because the differential airmass corrections within a CCD frame are negligible. The time-variable term was dropped because of its demonstrated small contribution to the final photometry (Suntzeff et al. 1999).

Once the MRO and APO images were bias subtracted and flattened, we obtained aperture magnitudes in the IRAF environment, using **phot** within the **apphot** package, and

calibrated the field stars using **mknoobsfile**, **fitparams**, and **evalfit** within the **photcal** package. The transformation equations were configured to produce V magnitudes, $B - V$, $V - R$, and $V - I$ colors. The APO infrared data were reduced using IRAF scripts written by Alan Diercks, and the IR mosaics were produced using Eugene Magnier’s image processing program **mana**. We then carried out aperture photometry within IRAF.

The mean optical transformation coefficients for the four optical systems described above are to be found in Table 1.

Figure 1 shows a combined BVR image taken with the CTIO 0.9-m telescope when SN 2000cx was on the rise. Some nearby field stars are marked. Optical photometry of these stars, obtained from imagery with YALO and MRO, is to be found in Table 2. A comparison of the independent YALO, MRO, and Li et al. (2001) values for the field stars marked as numbers 2, 4, and 8 in Fig. 1 shows good agreement. The *range* of the mean values for these three stars is 16-29 mmag in B , 12-17 mmag in V , 14-30 mmag in R , and 6-36 mmag in I , respectively. Thus, photometry of *stars* can be carried out at the $\sim 0^m02$ mag level.

Absolute calibration in J , H , and K was done via observations of the SN 2000cx field along with infrared standards of Persson et al. (1998), using the LCO Swope 1-m telescope on five nights in October and November 2001. The mean JHK values for field stars 1 and 2 are given in Table 2. Because of the size of the field of view of the IR camera on the APO 3.5-m telescope, only star 1 and SN 2000cx were always on the chip while dithering. To make the fullest use of all the nights when IR data were taken (i.e. photometric and non-photometric nights), we chose to reduce all our IR photometry of SN 2000cx (i.e. from YALO *and* APO) with respect to field star 1.

Our infrared YALO images were reduced using a package of scripts written by one of us (NBS),² which runs in the IRAF environment. This package contain tasks which fill out the file headers with information necessary for subsequent reduction and take care of bias correction, field flattening, masking out bad pixels, and vignetting. Fortunately, field star number 1 and the SN were located out of the zone of vignetting so that we did not have to worry about that at all. A section free of stars was chosen for each night so we could calculate a clean sky level and subtract that from all individual frames.

Tables 3 through 6 contain our optical data from the CTIO 0.9-m, YALO, APO, and MRO telescopes, respectively. In effect, we have four independent optical datasets, with two independent calibrations. The uncertainties of the values in the tables derive from photon statistics and the uncertainties of color corrections, and are to be considered minimum

²<http://www.ctio.noao.edu/nick/reduction/reduction.html>

internal errors. A more accurate estimate of the accuracy of our photometry is obtained by fitting fourth order polynomials to the light curves, telescope by telescope and filter by filter, to measure the RMS residuals of such fits, under the assumption that the variation of light of the SN is a smooth function for each filter. We have calculated these residuals for our two largest datasets, using data prior to 25 d after the time of B -band maximum. For the YALO data the internal errors are $\sigma_B = \pm 14$; $\sigma_V = \pm 34$; $\sigma_R = \pm 41$; and $\sigma_I = \pm 71$ mmag. For the MRO data the internal errors are $\sigma_B = \pm 6$; $\sigma_V = \pm 20$; $\sigma_R = \pm 43$; and $\sigma_I = \pm 51$ mmag.

Figure 2 shows our optical data. Fig. 3 is the same as Fig. 2, but with the addition of the KAIT and Wise Observatory data given by Li et al. (2001), plus data obtained by Jha (2002) with the 1.2-m telescope at the Fred L. Whipple Observatory at Mt. Hopkins, Arizona.

There are systematic differences between different subsets of the data. With the sense of $\Delta \equiv$ “YALO *minus* MRO”, at the time of B -band maximum $\Delta B = -0.04$, $\Delta V = -0.05$, $\Delta R = -0.04$, $\Delta I = +0.05$ mag. At $t = 17.4$ d, from Tables 4 and 6 we find $\Delta B = -0.02$, $\Delta V = -0.08$, $\Delta R = -0.15$, $\Delta I = +0.16$ mag. The disagreement in V , R , and I is large.

Now, with the sense of $\Delta \equiv$ “CTIO 0.9-m *minus* MRO”, for the data within 7 days of maximum we find $\Delta B = -0.02$, $\Delta V = -0.04$, $\Delta R = -0.05$, $\Delta I = 0.00$ mag. This is not a significant improvement on the YALO vs. MRO situation *at maximum*. However, YALO photometry vs. CTIO 0.9-m data within a week of maximum is in agreement at the 0^m02 level or better for B , V , and R . In spite of systematic differences between datasets obtained with different telescopes and different filters, at least we know the apparent magnitudes at maximum to ± 0.03 mag.

The systematic differences in the photometry are undoubtedly due to differences in the actual filters used, coupled with the non-stellar spectral energy distribution of the SN. Very late-time I -band data are particularly discordant, more than 0.7 mag (KAIT vs. FLWO). Though some of the optical spectra discussed by Li et al. (2001) cover the full I -band (at 2, 6, 7, 32, 42 days after $T(B_{max})$ and later), to reconcile all data of SN 2000cx taken with different telescopes is beyond the scope of this paper.³

³Stritzinger et al. (2002) attempted to correct data of SN 1999ee obtained with multiple telescopes by calculating “S-corrections” using the spectra of this object plus knowledge of the filter transmission curves, quantum efficiencies of the chips, and appropriate atmospheric transmission functions. In the end they decided to leave their data uncorrected. However, more recently Krisciunas et al. (2003) derived corrections to their photometry of SN 2001el and applied the filter corrections to the $BVJHK$ data. This in particular solved problems with the B -, V -, J -, and H -band data. However, they found that R -band corrections were

Tables 7 and 8 contain the infrared data from YALO and APO, respectively. Table 9 has corrections to place the APO data (which are fewer in number) on the YALO filter system, using the method of Stritzinger et al. (2002) and Krisciunas et al. (2003). To our knowledge, only two infrared spectra of SN 2000cx itself exist (Rudy et al. 2002), and these were taken 6 and 7 days, respectively, before the observed date of B -band maximum. To calculate the filter corrections for the APO data of SN 2000cx we used the infrared spectra of SN 1999ee (Hamuy et al. 2002). In Figs. 4 and 5 we show our infrared photometry without, and with, the filter corrections. The agreement of the J -band datasets is clearly better with the corrections.

Finally, in Table 10 we give the times of maximum, as observed by us in the different bands. Our time of B -band maximum is 0.3 d later than that found by Li et al. (2001), well within the uncertainty. While they found that the V -band maximum occurred 2.1 d after B -band maximum, we find a lag of only 1.2 d. However, this difference is not statistically significant.

Jha (2002) also obtained $UBVRI$ photometry of SN 2000cx, though with a large gap in time after maximum. Late time photometry (10 July 2001) with HST , using the $F675W$ and $F814W$ filters, is given by Li et al. (2002). Altogether, the photometric database of SN 2000cx amounts to 642 data points. To our knowledge it is the largest dataset ever obtained for a Type Ia SN.

3. General Discussion

A vast majority of the light curves of Type Ia SNe can be fit into a classification scheme in which the shape of the light curves is correlated with the intrinsic luminosity of the SN (Phillips 1993, Riess, Press, & Kirshner 1996, Perlmutter et al. 1997, Phillips et al. 1999). Li et al. (2001) remark that the Multi-color Light Curve Shape (MLCS) fit to their data for SN 2000cx is the worst fit they have ever seen. SN 2000cx was a reasonably fast riser, but a slow decliner. That would mean that the “stretch factor” used with the method of Perlmutter et al. (1997) would give a different value prior to maximum compared to after maximum. Since the stretch factor in B and V is related to the intrinsic luminosity, how does one determine the intrinsic luminosity of this SN?

NGC 524, the host galaxy of SN 2000cx, has had its distance modulus measured via

not really necessary, and that applying I -band corrections actually made datasets obtained with different telescopes much *more* discordant.

the Surface Brightness Fluctuation (SBF) method. Tonry et al. (2001) obtain $m - M = 31.90 \pm 0.20$ for the distance modulus. Li et al. (2001) obtained $m - M = 32.53 \pm 0.35$ using MLCS. Using the corrected recession velocity of NGC 524 in the Local Group frame of 2192 km s^{-1} and a Hubble constant of $74 \text{ km s}^{-1} \text{ Mpc}^{-1}$, in agreement with the *HST* Key Project value (Freedman et al. 2001), we obtain a distance modulus of 32.36 mag.

SN 2000cx was located in the outer regions of an early-type galaxy. Since early-type galaxies contain minimal amounts of dust, and the $B - V$ colors of SN 2000cx were particularly blue, we explicitly assume that this SN was unreddened in its host. We shall correct for reddening due to dust in our Galaxy (see below).

Krisciunas et al. (2003) showed that the H -band absolute magnitudes of Type Ia SNe 10 days after the time of B -band maximum appear to be a flat function of the decline rate $\Delta m_{15}(B)$. For a sample of 9 objects with $\Delta m_{15}(B) < 1.3$ they found a mean H -band absolute magnitude of -17.91 ± 0.05 . The observed H -band magnitude of SN 2000cx 10 days after B -band maximum is 14.64 ± 0.04 . From the Galactic reddening maps of Schlegel, Finkbeiner, & Davis (1998), we estimate that the color excess $E(B - V) = 0.082$ mag in the direction of SN 2000cx. Using the interstellar extinction model of Rieke & Lebofsky (1985), we estimate that the H -band extinction, due only to the effect of dust in our Galaxy, is 0.04 mag. Assuming that the absolute magnitude of SN 2000cx is also -17.91 , given its corrected H -band magnitude of 14.60, we obtain a distance modulus $m - M = 32.51$. Thus, the distance moduli from MLCS, Hubble’s Law, and the H -band analysis are in reasonable agreement, with an unweighted mean value of 32.47 ± 0.05 , corresponding to a distance of 31 ± 1 Mpc.

Given the observed V -band maximum of 13.25, $A_V \approx 3.1 \times 0.082 = 0.25$, and a distance modulus of 32.47, the implied V -band absolute magnitude of SN 2000cx is -19.47 , which is comparable to the mean of M_V of the slow decliners (Krisciunas et al. 2003, Fig. 13).

However, Ajhar et al. (2001) have shown that there is excellent agreement between distance determinations using SBF and other methods. The host of SN 2000cx is actually a bit close ($cz < 3000 \text{ km s}^{-1}$) to derive its distance via Hubble’s Law. The MLCS distance can also be doubted because the light curves cannot be fit well using MLCS templates. Also, on the basis of a larger sample of objects, it may turn out that H -band absolute magnitudes do show some kind of decline rate relation. In that case, should we use the *decline* rate of SN 2000cx or some modified value that takes into account its different rise and decline rates?

Let us assume that the Tonry et al. (2001) distance modulus of $m - M = 31.90 \pm 0.20$ is correct. On an $H_0 = 74$ scale this would be $m - M = 31.84$ mag. Adopting $A_B = 0.34$, $A_V = 0.25$, and $A_I = 0.12$ mag and the maximum magnitude values given in Table 10, we obtain

absolute magnitudes of $M_B = -18.76$, $M_V = -18.84$, $M_I = -18.31$, with uncertainties of ± 0.20 mag. These correspond to $\Delta m_{15}(B)$ in the range 1.4-1.7 (Krisciunas et al. 2003, Fig. 13). M_H ($t = 10$ d) would be -17.24 , comparable to that of SN 2000bk, which was a fast decliner with $\Delta m_{15}(B) = 1.63$.

Krisciunas et al. (2001, Figs. 16 and 17) devised a quantitative measure of the strength of the I -band secondary hump common to Type Ia SNe, namely the mean flux-with-repect-to-maximum from 20 to 40 d after the time of B -band maximum. They found that 90 percent of Type Ia SNe have values of $\langle I \rangle_{20-40}$ that are well correlated with the B -band decline rate $\Delta m_{15}(B)$. There were two exceptions to the rule, showing that there can be objects with identical decline rates in B and V but much stronger or weaker secondary humps in I . For SN 2000cx we find that $\langle I \rangle_{20-40} = 0.35$. This would imply $\Delta m_{15}(B) \approx 1.7$ like the fast decliners SNe 1992bo or 1993H. But SN 2000cx is a slow decliner, with $\Delta m_{15}(B) = 0.93$. If we were to add a point in Fig. 17 of Krisciunas et al. (2001) corresponding to SN 2000cx, it would be the most discrepant point in the graph.

Li et al. (2001) point out that the stretch factor for the pre-maximum data points ($t = -8$ to 1 day) corresponds to $\Delta m_{15}(B) = 1.64 \pm 0.02$. In various ways SN 2000cx masquerades as a fast Type Ia SN and also as a slow one.

One of the patterns exhibited by many unreddened Type Ia SNe is that their $B - V$ colors from 30 to 90 d after the time of V -band maximum follow a particular linear trend, whether they are fast-decliners or slow-decliners (Lira 1995, Phillips et al. 1999). Li et al. (2001) and Cuadra et al. (2001) noted that SN 2000cx was roughly 0.2 mag bluer than the Lira line. In Fig. 6 we show the $B - V$ data from YALO, the CTIO 0.9-m, APO, and MRO telescopes. The data have been dereddened by 0.082 mag to account for dust in our Galaxy (Schlegel et al. 1998). The data after JD 2,451,784 are, on average, 0.217 mag below the Lira line. We assume, because SN 2000cx occurred in the outer regions of an early-type galaxy, that it suffered no host reddening. But if its light was affected by dust in the host galaxy, then the points in Fig. 6 should be displaced even further below the Lira line. Truly, the $B - V$ colors of this SN are unusual.

In Figs. 7, 8, and 9 we show the JHK light curves of SN 2000cx along with data of other objects: SNe 1999aw (Strolger et al. 2002), 2001el (Krisciunas et al. 2003), 1999ac (Phillips et al. 2002, 2003), 2000bk (Krisciunas et al. 2001), and 1986G (Frogel et al. 1987). The light curves are ordered from top to bottom by the decline rate $\Delta m_{15}(B)$.

We the note the extremely deep dip in the J -band in the 20 days after maximum. We also note the similarity of the SN 2000cx J -band data with that of SN 2000bk, a fast decliner. The latter had an earlier secondary J -band maximum, however. We also note, whereas most

Type Ia SNe have relatively flat H - and K -band light curves in the 20 days after maximum, SN 2000cx showed decreasing flux at this epoch.

Krisciunas et al. (2000, 2001, 2003) found that Type Ia SNe which are *mid-range* decliners appear to exhibit uniform V minus infrared color curves from about one week before maximum until three or more weeks after maximum. They asserted that the unreddened loci can be used to derive the total extinction suffered by the light of a Type Ia SN on its way to our viewing location in the Galaxy. They found that $V - H$ and $V - K$ were particularly well behaved, and modelling by Höflich given in Krisciunas et al. (2003) confirms this observational result from a theoretical standpoint. Krisciunas et al. (2000, 2001) also noted that fast decliners and slow decliners have different unreddened loci. The slow decliners have bluer loci, and the fast decliners have redder loci.

Using data of the slow decliners SNe 1999aa (Krisciunas et al. 2000), 1999aw (Strolger et al. 2002), and 1999gp (Krisciunas et al. 2001), which appear to be unreddened in their hosts, we can correct the $V - J$, $V - H$, and $V - K$ colors for the effect of dust in our Galaxy (Schlegel et al. 1998) and construct unreddened loci for slowly declining Type Ia SNe. We also used the optical data of SN 1999ee (Stritzinger et al. 2002) along with some unpublished IR data of SNe 1999ee and 2001ba taken at Las Campanas Observatory and CTIO to constrain the shape of the unreddened loci.

Following Krisciunas et al. (2000), let t equal the number of days since the time of B -band maximum, and T_c be some “crossover time” when the slope in the color curve has a sudden change. We consider only the data from $-9 < t < 27$ d and construct the simplest form of unreddened loci that can fit the data. For $V - J$ we have:

$$V - J = a_0 + a_i + b_1 (t - T_c) + c (t - T_c)^2 ; (t < T_c) . \quad (1)$$

$$V - J = a_0 + a_i + b_2 (t - T_c) ; (t \geq T_c) . \quad (2)$$

Each supernova has its own a_i value, but the objects presumed to be unreddened and which are used to establish the unreddened locus will have $\langle a_i \rangle = 0$. Reddened objects have $a_i > 0$. Under the assumption that the color curves of a group of unreddened supernovae are validly parameterized by a uniform locus, and that the reddened objects exhibit the same locus simply shifted to the red, the goal is to use all the data for a given color index to solve for the crossover time, the zeropoint, the slopes, the second order coefficient, and the color excesses of each reddened object.

In Fig. 10 we show the unreddened $V - J$ color locus for slowly declining Type Ia SNe.

Using the $B - V$ color excesses given by Schlegel et al. (1998) and $E(V - J) = 2.223 E(B - V)$ from a standard model of Galactic dust (Rieke & Lebofsky 1985), we have subtracted $V - J$ color excesses of 0.089, 0.072, and 0.124 mag, respectively, from the observed $V - J$ colors of SNe 1999aa, 1999aw, and 1999gp. We assume that these three objects were unreddened in their host galaxies. For SN 1999ee we derive $E(V - J) = 0.658 \pm 0.022$. This has been subtracted from the SN 1999ee data shown in Fig. 10. The $V -$ near IR color loci given by Krisciunas et al. (2000) were not extrapolated beyond $t = 27$ d, and we have truncated our $V - J$ locus at that epoch, though on the basis of SN 1999aw we might have extended the right-hand line further.

The $V - J$ photometry of slowly declining Type Ia SNe gives a crossover time $T_c = 14.43 \pm 0.33$ d. We find $a_0 = -1.96$, $b_1 = -0.07480 \pm 0.00747$ mag d⁻¹, $c = -0.00015 \pm 0.00030$ mag d⁻², and $b_2 = 0.06867 \pm 0.00500$ mag d⁻¹. Whereas the c term was necessary for the mid-range decliners studied by Krisciunas et al. (2000), we found that it was not statistically significantly different than zero for the slow decliners. We list it here only for reasons of completeness.

Given the optical color excess $E(B - V) = 0.082$ for SN 2000cx and the interstellar extinction law quantified by Rieke & Lebofsky (1985), we estimate the following color excesses: $E(V - J) = 0.182$; $E(V - H) = 0.210$; and $E(V - K) = 0.226$.

In Fig. 11 we show the dereddened $V - J$ colors of SN 2000cx, along with the unreddened color locus described above (the solid line). We also show for reference (as a dashed line) the unreddened color locus for mid-range decliners given by Krisciunas et al. (2000). The big dip observed in the J -band leads to a very blue $V - J$ color for SN 2000cx at $t = 10$ d. However, the $V - J$ colors match the unreddened locus for slow decliners overlapping the time of maximum light. We note that conversion of the J -band data to the filter system of Persson et al. (1998) would make our data up to 0^m07 fainter at maximum light, assuming that the IR spectral evolution of SN 2000cx was similar to SN 1999ee (see Krisciunas et al. 2003, Fig. 6). This would make the $V - J$ data shown on the left hand side of Fig. 11 up to 0^m07 bluer.

A similar analysis of the $V - H$ colors of SNe 1999aw, 1999gp, and 1999ee gives a crossover time $T_c = 5.71 \pm 0.27$ d, $a_0 = -1.60$, $b_1 = -0.06872 \pm 0.00304$ mag d⁻¹, $c \equiv 0$, and $b_2 = 0.07502 \pm 0.00262$ mag d⁻¹. In this case we have subtracted $E(V - H) = 0.083$ mag from the observed colors of SN 1999aw and 0.143 mag from the data of SN 1999gp, to account for the effect of dust in our Galaxy. We derived a total color excess of $E(V - H) = 0.795 \pm 0.023$ for the reddening of SN 1999ee. The $E(V - J)$ and $E(V - H)$ color excesses of SN 1999ee are consistent with one unique value (rather than two disjoint values) of $A_V = 0.944 \pm 0.061$, which is a good consistency check relating to the assumption that there exist

uniform color loci.

In Fig. 12 we show a corresponding plot for dereddened $V - H$ colors of SN 2000cx, with the unreddened loci for slow decliners (solid line) and mid-range decliners (dashed line) shown. For $V - H$ there is good agreement between the SN 2000cx data and the unreddened locus for slow decliners from $t = 10$ to 27 d. Conversion of the H -band data to the filter system of Persson et al. (1998) would change the data from $10 < t < 27$ d by up to 0^m06 , making them brighter, and the $V - H$ colors redder. Once again, this assumes that the IR spectral evolution of SN 2000cx was similar to that of SN 1999ee.

In Fig. 13 we show the $V - K$ data of SN 2000cx, corrected only for the reddening due to our Galaxy, along with dereddened data of SNe 1999aa, 1999ee, 1999gp, and 2001ba. The $V - K$ colors of SN 2000cx are quite similar to these other slow decliners, both pre- and post-maximum. From $10 < t < 21$ d SN 2000cx is the bluest object in this color index.

4. The Bolometric Behavior of SN 2000cx

The wide wavelength coverage of the $UBVRIJHK$ broadband magnitudes allows us to construct ultraviolet/optical/near-infrared “uvoir” bolometric light curves. Only a few papers have been published trying to estimate the bolometric light curves of Type Ia supernovae. (See Leibundgut & Suntzeff 2003 for a summary.) The calculated luminosities are not the true bolometric luminosities, but represent the fraction of the gamma rays produced in the radioactive decays of the synthesized nuclides that are thermalized in the expanding debris nebula. As shown by Leibundgut & Pinto (1992) and Leibundgut (2000), a significant fraction of the gamma rays leak out of the supernova debris going from 10 percent at the time of B_{max} to over 50 percent 40 days after maximum.

Suntzeff (1996) used ultraviolet spectra, optical $UBVRI$, and near-infrared JHK data to estimate accurate bolometric fluxes. Because of the limited infrared data at the time, only a few points on the bolometric light curves could be accurately calculated. Vacca & Leibundgut (1996) and Contardo, Leibundgut, & Vacca (2000) obtained more complete uvoir bolometric light curves by integrating optical broad-band magnitudes. Applying Arnett’s law (Arnett 1982) to the peak bolometric luminosities, Vacca & Leibundgut (1996) and Contardo et al. (2000) found a range of more than a factor in 10 in the ^{56}Ni masses for a group of nearby Type Ia SNe. Cappellaro et al. (1997) used a V magnitude with a bolometric correction to study the gamma-ray trapping in the late-time light curves, which also showed a significant range in ^{56}Ni masses.

We have integrated the broad-band magnitudes for SN 2000cx using a simple trapezoidal

rule and a conversion of broad-band to monochromatic fluxes from Suntzeff & Bouchet (1990). We have added extrapolations to the ultraviolet from the U filter and to the mid-infrared from the K or H filter using an extrapolation scheme discussed by Suntzeff (2003). These extrapolations only add ~ 2 percent for the missing infrared flux, and less than 10 percent for the ultraviolet after maximum light. In Fig. 14 we plot the uvoir bolometric luminosity for SN 2000cx. For comparison, we also plot similar data for SN 2001el and SN 1999ee taken from Suntzeff (2003). (Note that the data have been offset slightly for plotting purposes.) The SN 1999ee and SN 2001el data were taken from Stritzinger et al. (2002) and Krisciunas et al. (2003) and are meant to represent “normal” Type Ia supernovae with $\Delta m_{15}(B)$ of 0.94 and 1.13, which are similar to the Δm_{15} value of SN 2000cx. We have assumed the following distance moduli and $B - V$ reddening, which are based on a distance scale of $H_0 = 74 \text{ km s}^{-1} \text{ Mpc}^{-1}$: SN 2000cx, (32.47,0.082); SN 1999ee, (33.21,0.30); SN 2001el, (31.26, 0.21).⁴ The bolometric light curves have been plotted relative to the time of peak bolometric luminosity (not B_{max}) which we estimated from the curves.

The only remarkable difference between SN 2000cx and the normal Type Ia’s as seen in Fig. 14 is the lack of the flux excess around day 30. This flux excess, which is associated with the secondary maxima in IJK and a “shoulder” in R was noted by Suntzeff (1996) and Contardo et al. (2000). Since the energy source for the bolometric luminosity and the optical depth to gamma rays are monotonically declining at that date, such an inflection in the bolometric luminosity must be associated with cooling mechanism and not the energy input to the nebula.

In Fig. 15 we can see the differences in the bolometric light curves more clearly. Here we plot smoothed representations of the bolometric light curves, and at the bottom of the panel, the bolometric light curve of SN 2000cx with respect to SN 1999ee and SN 2001el. It can be seen that SN 2000cx rises to maximum more quickly and falls more quickly (within 10 days of maximum), but the effect is rather small. However, starting around day 25, SN 2000cx suddenly declines rapidly compared to these two SNe, reaches a maximum flux deficit around day 35, and then increases in brightness slightly to day 50. Fig. 15 gives the impression that the post-maximum flux enhancement of SN 2000cx was weaker and earlier than the comparison Type Ia events.

Two explanations for the secondary maximum have been published. One explanation for the secondary IJK maxima has been given by Pinto & Eastman (2000a, 2000b) who

⁴A systematic error of Δm in the distance modulus corresponds to a change in $\log(L)$ of $0.4 \times \Delta m$. If the true distance modulus of SN 2000cx is 31.90, then we must shift the bolometric light curve of SN 2000cx in Figs. 14 and 15 down by 0.228 mag.

note that this flux enhancement is due to a rapid change in the flux mean opacity. After maximum light, the thermalized energy input to the light curve from the radioactive nuclides is less than the observed luminosity, implying qualitatively that the post-maximum luminosity is powered by a reservoir of previously trapped radiation. If the post-maximum opacity decreases due to a drop in the effective temperature, the diffusion times drop and the trapped energy escapes more rapidly leading to a pause in the rapid luminosity decline. This bolometric flux excess appears in the redder colors because the opacities are very low and there are ample emission sources such as Fe II and Ca II.

A similar explanation has been given by Höflich (1995) and Höflich, Khokhlov, & Wheeler (1995). They note that the infrared luminosity can be roughly approximated by the Rayleigh-Jeans limit, namely:

$$(L_{IR-color}) \propto R_{ph}^2 T_{eff} D_{IR} \quad (3)$$

Here R_{ph} , T_{eff} , and D_{IR} are the photospheric radius, the effective temperature, and a dilution factor appropriate for a scattering dominated atmosphere. They argue that D_{IR} is a slowly varying function during this epoch. They show that after maximum, T_{eff} drops as the energy source switches from ^{56}Ni to ^{56}Co which starts the steep post-maximum decline. In many of their models however, the photospheric radius R_{ph} increases as it is dragged out by the expansion of the debris. Depending on the rate of expansion of the photosphere, this can cause the product in the equation for $L_{IR-color}$ to increase. The appearance of an expanding photosphere can only be maintained if the opacities stay high. In these conditions, as the photosphere is pulled outward with the debris, the luminosity will increase if T_{eff} does not drop dramatically. This high rate of cooling, which greatly exceeds the energy input from the radioactive nuclides, cannot be maintained indefinitely, and at some point the opacities will begin to drop so rapidly that apparent photospheric radius will also begin to recede quickly causing a sudden decrease in luminosity.

According to the models discussed above, this would support the hypothesis that SN 2000cx is a sub-luminous event. The sub-luminous SNe 1992A, 1992bo, and 1991bg (Contardo et al. 2000; see their Figure 5) also have weak or no secondary flux enhancements and SN 2000cx clearly belongs to this class.

Unfortunately, given the large number of unknown parameters in the models for the explosions of Type Ia SNe, this is not a strong conclusion. Pinto & Eastman (2000b) note that the secondary maximum is a sensitive function of how the much of the radioactive nuclides are mixed in the expanding debris from the core. An unusual mixing event bringing relatively more ^{56}Ni out from the core qualitatively could account for the lack of the secondary

flux enhancement independent of the intrinsic luminosity.

Returning to the empirical bolometric light curve, we find two other aspects of the morphology of the bolometric light curve which point to this event being sub-luminous. Contardo et al. (2000) showed that the decline rate between days 50 and 80 for their sample of Type Ia supernovae was 2.6 ± 0.1 mag per 100 days, except for most sub-luminous event in their sample, SN 1991bg, which had a decline rate of 3.0 mag per 100 days. SN 2000cx declined at 2.9 mag per 100 days during this time period. If one looks at their Fig. 5, one can also see that SN 1991bg also stands out in the peak-to-tail luminosity difference. In Fig. 16 we plot the difference in luminosity between the peak luminosity and 90 days after peak for the sample studied by Contardo et al. (2000). Evidently, this luminosity difference is correlated with $\Delta m_{15}(B)$, with the fainter SNe having larger luminosity differences. The observed value of this luminosity difference in SN 2000cx of 1.63 associates it with the sub-luminous group. This is also seen in Fig. 15 where this SN is compared to SNe 2001el and 1999ee. In that figure, the luminosity on the exponential tail for days beyond 50 are underluminous by about 0.2dex with respect to SN 2001el, which has a value of $\Delta m_{15}(B)$ of 1.13.

By day 50 or so, the energy deposition in a typical Type Ia supernova due to the thermalization of gamma rays occurs in regions which are optically thin in the optical and near-infrared (Pinto & Eastman 2000a). Thus, the luminosity at this epoch responds rapidly to the input energy source, which at this time is ^{56}Co . At maximum light, according to Arnett’s law, the bolometric luminosity equals the instantaneous energy input from the radioactive nuclides. The ratio of these two luminosities should then be independent, to first order, of the mass of ^{56}Ni synthesized.

The larger luminosity difference between the peak and 90 days after peak is thus caused by a smaller optical depth to gamma rays at late times. This could be caused, for instance, by positron escape as discussed by Milne, The, & Leising (2001) but the modelling shows minimal effects of positron trapping at this epoch due to the short positron lifetimes which approximate in situ deposition of positron energy. A lower optical depth to gamma rays could also be caused by an asymmetric mass distribution of the ejecta. Perhaps the simplest way to lower the optical depth is to increase the kinetic energy due to the explosion.

It is not unreasonable that the initial kinetic energy may be only vaguely related to the mass of ^{56}Ni synthesized. Pinto & Eastman (2000a; see their Figure 4), showed that a *larger* kinetic energy will lead to a more rapid decline in the mass column depth, and produce a narrower bolometric light curve and increased the peak-to-tail luminosity difference. In a subsequent article, Pinto & Eastman (2001) note that the explosion kinetic energy is not necessarily a function of the ^{56}Ni mass, since the total energy of the burning of a C/O mixture

is nearly the same if it burns to the Si group or to ^{56}Ni . The thermal energy liberated at the explosion does go entirely to the kinetic energy, but that kinetic energy may not be strongly coupled to the ^{56}Ni , which powers the subsequent light curve. Li et al. (2001) found that SN 2000cx did have very high sulfur and silicon velocities compared to SN 1994D, and also concluded that SN 2000cx may have had a larger than typical kinetic energy.

Thus, if the SBF distance is correct, a working hypothesis to explain the bolometric behavior of SN 2000cx is that this supernova is an *underluminous event with higher than normal kinetic energy*. We should not be too forceful in stressing this conclusion however. This event was clearly unusual in its color evolution, and simple morphological arguments may fail if model parameters, such as the extent of mixing of the radioactive nuclides or the symmetry of the explosion, are uncoupled from the other fundamental parameters such as the amount of ^{56}Ni synthesized. None of the evidence here clearly points to a shorter or longer distance to this supernova. Obviously, we need a better distance to NGC 524 to resolve this question.

5. Conclusions

SN 2000cx, the brightest supernova discovered in the year 2000, occurred in the unobscured outer regions of an early-type galaxy and was well observed with multiple telescopes, allowing us to compile a dataset of unprecedented size. While many Type Ia SNe have light curves that follow patterns that are now well established, SN 2000cx did not conform to these patterns.

SN 2000cx was a reasonably fast riser in B and V . From the pre-maximum photometry Li et al. (2001) obtain a stretch factor that corresponds to $\Delta m_{15}(B) = 1.64 \pm 0.02$. Based solely on its weak I -band secondary hump, we would have predicted $\Delta m_{15}(B) \approx 1.7$. If the distance modulus based on Surface Brightness Fluctuations of the host galaxy is correct (Tonry et al. 2001), the corresponding absolute magnitudes in $BVIH$ are comparable to fast decliners, with $\Delta m_{15}(B)$ in the range 1.4 to 1.7.

However, SN 2000cx was a slow *decliner*, with $\Delta m_{15}(B) = 0.93$. Its pre-maximum spectrum showed strong Fe III and weak Si II, like other slow decliners such as SN 1991T. Its $V - K$ color evolution, both pre- and post-maximum, was very similar to that of other slow decliners.

The bolometric behavior of SN 2000cx, when compared to the normal SNe 1999ee and 2001el, showed that this SN rose and fell from maximum light more rapidly, and that the magnitude difference between peak brightness and 90 days past peak was larger than

normal. This behavior is consistent with the higher kinetic energies seen at maximum light and reported by Li et al. (2002), but it can also be explained by this event being sub-luminous.

The distance modulus of SN 2000cx is somewhat problematic. We note, however, that MLCS (Riess et al. 1996, 1998), Hubble Law’s (with $H_0 = 74 \text{ km s}^{-1} \text{ Mpc}^{-1}$), and the method that uses the H -band absolute magnitude at $t = 10 \text{ d}$ (Krisciunas et al. 2003) give just about the same value. The SBF method gives a distance modulus roughly 0.6 mag smaller.

Given: 1) the accuracy of the photometry of SN 2000cx at maximum ($\pm 0.03 \text{ mag}$); 2) the host extinction of SN 2000cx is minimal (or zero); 3) the uncertainty of the Galactic extinction correction is also small; and 4) the light curves cannot be fit by templates based on other objects, confidently placing this SN in a Hubble diagram depends significantly on a direct measure of the host galaxy’s distance (such as with the SBF method) or on an absolute magnitude derived from an explosion model that can match the many unusual observed facts.

Support for Proposal Number GO-07505.02A, GO-08177.6, and GO-08641.07A was provided by NASA through a grant from the Space Telescope Science Institute, which is operated by the Association of Universities for Research in Astronomy, Inc., under NASA contract NAS5-26555. This paper is based, in part, on observations obtained with the Apache Point Observatory 3.5m telescope, which is owned and operated by the Astrophysical Research Consortium.

We thank W. D. Li for sharing the KAIT data considerably ahead of publication. We thank M. R. Garcia, L. Clark, D. Hoard, J. Alfonso, and K. Vivas for obtaining some of the data at CTIO. C. Stubbs, G. Miknaitis, and E. Bergeron helped with data acquisition for some APO observations. D. Edgeworth helped with some of the MRO observations. The APO infrared data were reduced using software written in part by A. Diercks and E. Magnier.

A. The R -band filter used at YALO

In Fig. 17 we show the filter transmission function of the R -band filter used with the YALO 1-m telescope for the observations presented here. This is a much more standard filter than that used by Stritzinger et al. (2002) for their observations of SN 1999ee using the same telescope and camera. Also shown in the diagram is the *effective* throughput in R , made up of the filter transmission function multiplied by an atmospheric transmission

function, the quantum efficiency of the chip, and two aluminum reflections. Both functions shown in Fig. 17 include a 280 Å shift to the blue, which comprises the 310 Å shift suggested by the manufacturer, taking into account the use of the filter when cooled, and a 30 Å shift back to red. This smaller shift was necessary to match the color term obtained for *R*-band photometry based on synthetic photometry with the actual color term derived from the observations of Landolt (1992) standards.

REFERENCES

- Ajhar, E. A., Tonry, J. L., Blakeslee, J. P., Riess, A. G., & Schmidt, B. P. 2001, *ApJ*, 539, 584
- Arnett, W. D. 1982, *ApJ*, 253, 785
- Cappellaro, E., Mazzali, P. A., Benetti, S., Danziger, I. J., Turatto, M., della Valle, M., & Patat, F. 1997, *A&A*, 328, 203
- Chornock, R., Leonard, D.C., Filippenko, A.V., Li, W. D., Gates, E.L. & Chloros, K. 2000, *IAU Circ.*, 7463
- Contardo, G., Leibundgut, B., & Vacca, W. D. 2000, *A&A*, 359, 876
- Cuadra, J., Suntzeff, N. B., Candia, P., Krisciunas, K., & Phillips, M. M. 2001, *BAAS*, 33, 1370
- Freedman, W., et al. 2001, *ApJ*, 553, 47
- Frogel, J. A., Gregory, B., Kawara, K., Laney, D., Phillips, M. M., Terndrup, D., Vrba, F., & Whitford, A. E. 1987, *ApJ*, 315, L129
- Hamuy, M., Maza, J., Pinto, P. A., et al. 2002, *AJ*, 124, 417
- Harris, W. E., Fitzgerald, M. P., & Reed, B. C. 1981, *PASP*, 93, 507
- Höflich, P. 1995, *ApJ*, 443, 89
- Höflich, P., Khokhlov, A. M., & Wheeler, J. C. 1995, *ApJ*, 444, 831
- Jha, S. 2002, Harvard University, Ph. D. Dissertation
- Krisciunas, K., Hastings, N. C., Loomis, K., McMillan, R., Rest, A., Riess, A. G., & Stubbs, C. 2000, *ApJ*, 539, 658

- Krisciunas, K., Phillips, M. M., Stubbs, C., et al. 2001, *AJ*, 122, 1616
- Krisciunas, K., Suntzeff, N. B., Candia, P., et al. 2003, *AJ*, in press (astro-ph/0210327)
- Landolt, A. U. 1992, *AJ*, 104, 340
- Leibundgut, B. 2000, *A&A Rev.*, 10, 179
- Leibundgut, B., & Pinto, P. A. 1992, *ApJ*, 401, 49
- Leibundgut, B., & Suntzeff, N. 2003, *Supernovae & GRBs*, ed. K. Weiler, (Springer-Verlag), in press
- Li, W. D., Filippenko, A. V., Gates, E., et al. 2001, *PASP*, 113, 1178
- Li, W. D., Filippenko, A. V., Van Dyk, S. D., Hu, J., Qiu, Y., Modjaz, M., & Leonard, D. C. 2002, *PASP*, 114, 403
- Lira, P. 1995, Master's thesis, Univ. of Chile
- Milne, P. A., The, L.-S., & Leising, M. D. 2001, *ApJ*, 559, 1019
- Perlmutter, S., et al. 1997, *ApJ*, 483, 565
- Persson, S. E., Murphy, D. C., Krzeminski, W., Roth, M., & Rieke, M. J. 1998, *AJ*, 116, 2475
- Phillips, M. M. 1993, *ApJ*, 413, L105
- Phillips, M. M., Lira, P., Suntzeff, N. B., Schommer, R. A., Hamuy, M., & Maza, J. 1999, *AJ*, 118, 1766
- Phillips, M. M., et al. 2002, in *From Twilight to Highlight – The Physics of Supernovae*, ESO/MPA/MPE Workshop, Garching, in press (astro-ph/0211100)
- Phillips, M. M., et al. 2003, in preparation
- Pinto, P. A. & Eastman, R. G. 2000a, *ApJ*, 530, 744
- Pinto, P. A. & Eastman, R. G. 2000a, *ApJ*, 530, 757
- Pinto, P. A. & Eastman, R. G. 2001, *New Astronomy*, 6, 307
- Rieke, G. H., & Lebofsky, M. J. 1985, *ApJ*, 288, 618
- Riess, A. G., Press, W. H., & Kirshner, R. P. 1996, *ApJ*, 473, 88

- Riess, A. G., Filippenko, A. V., Challis, P., et al. 1998, AJ, 116, 1009
- Rudy, R. J., Lynch, D. K., Mazuk, S., Venturini, C. C., Puetter, R. C., & Höflich, P., ApJ, 565, 413
- Schlegel, D. J., Finkbeiner, D. P., & Davis, M. 1998, ApJ, 500, 525
- Stetson, P. 1987, PASP, 99, 191
- Stetson, P. 1990, PASP, 102, 932
- Stritzinger, M., Hamuy, M., Suntzeff, N. B., et al. 2002, AJ, 124, 2100
- Strolger, L.-G., Smith, R. C., Suntzeff, N. B., et al. 2002, AJ, 124, 2905
- Suntzeff, N. B. & Bouchet, P. 1990, AJ, 99, 650
- Suntzeff, N. B. 1996, IAU Colloq. 145, Supernovae and Supernova Remnants, 41
- Suntzeff, N.B. 2003, From Twilight to Highlight - The Physics of Supernovae” ESO/MPA/MPE Workshop, Garching.
- Suntzeff, N. B., Phillips, M. M., Covarrubias, R., et al. 1999, AJ, 117, 1175
- Tonry, J. L., Dressler, A., Blakeslee, J. P., Ajhar, E. A., Fletcher, A. B., Luppino, G. A., Metzger, M. R., & Moore, C. B. 2001, ApJ, 546, 681
- Vacca, W. D. & Leibundgut, B. 1996, ApJ, 471, L37
- Yu, C., Modjaz, M., & Li, W. D. 2000, IAU Circ., 7458

Table 1. Average Photometric Transformation Values^a

Parameter	Color Term	Mean Error	Color Index	Extinction	Mean Error
YALO 1-m (3 nights)					
<i>B</i>	−0.079	0.003	<i>B</i> − <i>V</i>	0.248	0.007
<i>V</i>	0.018	0.003	<i>B</i> − <i>V</i>	0.131	0.005
<i>R</i>	−0.030	0.005	<i>V</i> − <i>R</i>	0.076	0.007
<i>I</i>	0.045	0.003	<i>V</i> − <i>I</i>	0.009	0.006
CTIO 0.9-m (7 nights)					
<i>U</i>	−0.076	0.016	<i>U</i> − <i>V</i>	0.443	0.054
<i>B</i>	0.126	0.009	<i>B</i> − <i>V</i>	0.236	0.018
<i>V</i>	−0.017	0.006	<i>B</i> − <i>V</i>	0.139	0.009
<i>R</i>	0.005	0.014	<i>V</i> − <i>R</i>	0.087	0.011
<i>I</i>	−0.007	0.009	<i>V</i> − <i>I</i>	0.048	0.012
MRO (15 nights)					
<i>V</i>	0.044	0.003	<i>b</i> − <i>v</i>	0.201	0.029
<i>B</i> − <i>V</i>	1.067	0.004	<i>b</i> − <i>v</i>	0.142	0.015
<i>V</i> − <i>R</i>	1.026	0.006	<i>v</i> − <i>r</i>	0.061	0.021
<i>V</i> − <i>I</i>	1.014	0.003	<i>v</i> − <i>i</i>	0.083	0.027
APO (9 nights)					
<i>V</i>	0.026	0.011	<i>b</i> − <i>v</i>	0.216	0.029
<i>B</i> − <i>V</i>	0.975	0.002	<i>b</i> − <i>v</i>	0.103	0.016
<i>V</i> − <i>R</i>	1.040	0.003	<i>v</i> − <i>r</i>	0.036	0.024
<i>V</i> − <i>I</i>	1.003	0.017	<i>v</i> − <i>i</i>	0.083	0.030

^aThe color terms for YALO and the CTIO 0.9-m scale standardized colors, while the color terms for APO and MRO scale instrumental colors.

Table 2. Photometry of Comparison Stars

ID	V	$B - V$	$U - B$	$V - R$	$V - I$
1 ^a	11.141 (0.001)	0.536 (0.002)	0.000 (0.004)	0.328 (0.004)	0.666 (0.002)
1 ^b	11.145 (0.005)	0.528 (0.011)	...	0.325 (0.011)	0.672 (0.010)
2 ^a	12.564 (0.002)	0.606 (0.011)	0.015 (0.021)	0.366 (0.002)	0.733 (0.004)
2 ^b	12.572 (0.004)	0.587 (0.006)	...	0.370 (0.009)	0.749 (0.007)
3 ^a	14.780 (0.005)	0.778 (0.012)	0.172 (0.038)	0.441 (0.007)	...
4 ^a	13.494 (0.003)	0.797 (0.004)	0.315 (0.006)	0.470 (0.004)	0.911 (0.005)
4 ^b	13.509 (0.003)	0.778 (0.008)	...	0.471 (0.007)	0.930 (0.007)
5 ^a	15.364 (0.007)	1.005 (0.017)	0.671 (0.050)	0.545 (0.009)	...
6 ^a	16.366 (0.005)	1.044 (0.017)	0.903 (0.072)	0.624 (0.007)	1.167 (0.007)
7 ^a	16.765 (0.007)	0.962 (0.014)	0.712 (0.176)	0.584 (0.009)	1.096 (0.009)
8 ^a	12.812 (0.006)	0.696 (0.011)	0.099 (0.022)	0.400 (0.007)	0.797 (0.008)
8 ^b	12.808 (0.005)	0.677 (0.008)	...	0.384 (0.024)	0.800 (0.006)
9 ^a	15.223 (0.003)	1.233 (0.013)	1.211 (0.041)	0.727 (0.005)	1.339 (0.005)
10 ^a	14.559 (0.003)	0.826 (0.009)	0.352 (0.022)	0.463 (0.005)	0.908 (0.004)
11 ^a	15.616 (0.008)	1.158 (0.022)	1.233 (0.086)	0.687 (0.010)	...
	J	H	K		
1 ^c	10.006 (0.006)	9.758 (0.008)	9.689 (0.008)		
2 ^c	11.974 (0.006)	11.585 (0.015)	11.501 (0.014)		

^aMean values from 7 nights of CTIO 0.9-m imagery. ^bMean values from 6 nights of MRO imagery. ^cMean values from 5 nights of LCO imagery.

Table 3. *UBVRI* Photometry of SN 2000cx. CTIO 0.9-m Data^a

JD+2451000	<i>U</i>	<i>B</i>	<i>V</i>	<i>R</i>	<i>I</i>	Observer
745.88	13.722 (0.011)	13.995 (0.007)	13.821 (0.004)	13.796 (0.006)	...	Leiton/Clark
749.84	13.223 (0.015)	13.517 (0.012)	13.380 (0.008)	13.443 (0.013)	13.617 (0.014)	Garcia
750.86	13.195 (0.011)	13.474 (0.008)	13.336 (0.005)	13.408 (0.056)	...	Garcia
751.85	13.190 (0.011)	13.442 (0.008)	13.294 (0.005)	13.380 (0.010)	13.672 (0.011)	Garcia
757.84	...	13.640 (0.008)	13.328 (0.005)	13.444 (0.007)	13.949 (0.011)	Hoard
824.70	...	17.134 (0.041)	16.672 (0.018)	16.583 (0.028)	17.018 (0.039)	Smith
825.71	17.342 (0.064)	17.157 (0.033)	16.687 (0.020)	16.622 (0.032)	17.103 (0.044)	Smith
826.67	17.394 (0.094)	17.226 (0.042)	16.720 (0.023)	16.651 (0.042)	17.140 (0.056)	Smith
827.72	...	17.225 (0.009)	16.752 (0.004)	...	17.175 (0.019)	Smith
834.65	...	17.356 (0.026)	16.938 (0.017)	...	17.490 (0.029)	Candia

^aThe uncertainties given are due to photon statistics and zeropoint errors only.

Table 4. *BVRI* Photometry of SN 2000cx. YALO Data^a

JD+2451000	<i>B</i>	<i>V</i>	<i>R</i>	<i>I</i>	Observer
744.90	14.158 (0.083)	14.116 (0.059)	13.973 (0.095)	14.037 (0.084)	D. Gonzalez
745.86	13.955 (0.008)	13.790 (0.005)	13.774 (0.016)	13.875 (0.011)	D. Gonzalez
750.88	13.419 (0.010)	13.288 (0.007)	13.369 (0.014)	13.643 (0.012)	D. Gonzalez
752.89	13.409 (0.015)	13.230 (0.006)	13.361 (0.032)	13.820 (0.076)	J. Espinoza
755.87	13.496 (0.009)	13.240 (0.007)	13.359 (0.019)	13.873 (0.014)	J. Espinoza
757.82	13.602 (0.018)	13.296 (0.010)	13.439 (0.020)	13.960 (0.016)	J. Espinoza
760.81	13.810 (0.066)	13.440 (0.017)	13.673 (0.029)	14.309 (0.040)	J. Espinoza
763.84	14.033 (0.007)	13.639 (0.003)	...	14.647 (0.020)	D. Gonzalez
766.83	14.305 (0.007)	13.862 (0.005)	14.165 (0.013)	14.798 (0.011)	J. Espinoza
769.84	14.602 (0.012)	14.061 (0.008)	14.265 (0.053)	14.777 (0.016)	J. Espinoza
772.74	14.915 (0.013)	14.234 (0.008)	14.301 (0.024)	14.656 (0.016)	D. Gonzalez
775.77	15.263 (0.023)	14.444 (0.016)	14.355 (0.046)	14.522 (0.036)	D. Gonzalez
781.77	15.958 (0.006)	15.001 (0.003)	14.758 (0.020)	14.640 (0.016)	J. Espinoza
784.77	16.191 (0.009)	15.232 (0.003)	14.970 (0.016)	14.881 (0.009)	J. Espinoza
791.75	16.491 (0.008)	15.583 (0.003)	15.332 (0.006)	15.355 (0.008)	D. Gonzalez
802.74	16.741 (0.028)	16.002 (0.018)	15.757 (0.039)	15.928 (0.030)	D. Gonzalez
805.83	16.777 (0.014)	16.084 (0.005)	15.873 (0.011)	16.081 (0.013)	D. Gonzalez
812.85	16.912 (0.007)	16.293 (0.004)	16.115 (0.010)	16.401 (0.010)	J. Espinoza
820.70	17.032 (0.018)	16.539 (0.010)	16.394 (0.017)	16.784 (0.019)	J. Alfonso
827.68	17.154 (0.020)	16.760 (0.009)	16.613 (0.014)	17.045 (0.016)	J. Espinoza/K. Vivas

^aThe uncertainties given are due to photon statistics and zeropoint errors only. From polynomial fits to the YALO data we estimate that the internal errors are greater than or equal to $\sigma_B = \pm 14$; $\sigma_V = \pm 34$; $\sigma_R = \pm 41$; and $\sigma_I = \pm 71$ mmag. See text for a discussion of systematic errors.

Table 5. *BVRI* Photometry of SN 2000cx. APO Data^a

JD+2451000	<i>B</i>	<i>V</i>	<i>R</i>	<i>I</i>	Observers
760.90	13.829 (0.005)	13.512 (0.002)	13.757 (0.003)	14.270 (0.005)	Krisciunas/McMillan
784.70	16.169 (0.014)	15.263 (0.004)	15.012 (0.010)	14.799 (0.010)	Rest/McMillan
788.71	16.336 (0.008)	15.473 (0.003)	15.214 (0.008)	15.081 (0.008)	Rest/Miknaitis/Hastings
822.75	17.066 (0.010)	16.635 (0.004)	16.515 (0.009)	16.861 (0.013)	Krisciunas/McMillan
834.61	...	16.976 (0.007)	...	17.299 (0.017)	Krisciunas/Bergeron

^aThe uncertainties given are due to photon statistics and zeropoint errors only.

Table 6. *BVRI* Photometry of SN 2000cx. MRO Data^a

JD+2451000	<i>B</i>	<i>V</i>	<i>R</i>	<i>I</i>	Observer
744.92	14.177 (0.017)	14.008 (0.007)	13.997 (0.011)	14.057 (0.015)	Tavener/Logan
745.93	13.975 (0.012)	13.814 (0.005)	13.788 (0.008)	13.869 (0.011)	Logan
752.88	13.444 (0.006)	13.281 (0.002)	13.409 (0.004)	13.719 (0.007)	Krisciunas
753.96	13.458 (0.007)	13.263 (0.003)	13.389 (0.004)	13.729 (0.009)	Thomas/Snider
754.97	13.487 (0.005)	13.265 (0.002)	13.384 (0.004)	13.757 (0.007)	Thomas/Snider
757.94	13.640 (0.006)	13.346 (0.002)	13.498 (0.004)	13.968 (0.006)	Tavener/Logan
758.94	13.695 (0.007)	13.380 (0.003)	13.558 (0.005)	14.039 (0.008)	Tavener/Logan
759.93	13.768 (0.006)	13.423 (0.003)	...	14.149 (0.008)	Krisciunas/Edgeworth
764.91	14.162 (0.007)	13.803 (0.003)	14.135 (0.005)	14.591 (0.009)	Tavener/Logan
765.96	14.250 (0.005)	13.887 (0.002)	14.219 (0.004)	14.636 (0.007)	Tavener/Logan
769.88	14.626 (0.007)	14.142 (0.003)	14.412 (0.006)	14.619 (0.008)	Krisciunas
776.91	15.424 (0.021)	14.639 (0.011)	14.516 (0.020)	14.494 (0.025)	G. Gonzalez/West
783.00	16.094 (0.028)	15.140 (0.012)	14.820 (0.023)	14.728 (0.034)	Tavener/Logan
784.95	16.166 (0.015)	15.284 (0.006)	15.033 (0.013)	14.788 (0.015)	Tavener/Logan
807.83	16.860 (0.017)	16.170 (0.007)	16.097 (0.020)	16.209 (0.018)	Krisciunas

^aThe uncertainties given are due to photon statistics and zeropoint errors only. From polynomial fits to the MRO data we estimate that the internal errors are greater than or equal to $\sigma_B = \pm 6$; $\sigma_V = \pm 20$; $\sigma_R = \pm 43$; and $\sigma_I = \pm 51$ mmag. See text for a discussion of systematic errors.

Table 7. *JHK* Photometry of SN 2000cx. YALO Data

JD+2451000	<i>J</i>	<i>H</i>	<i>K</i>	Observer
744.89	14.280 (0.009)	14.378 (0.017)	14.324 (0.031)	D. Gonzalez
745.86	14.118 (0.008)	14.123 (0.008)	14.254 (0.024)	D. Gonzalez
750.87	13.900 (0.007)	14.071 (0.014)	13.949 (0.022)	D. Gonzalez
752.89	14.052 (0.008)	14.241 (0.016)	14.112 (0.025)	J. Espinoza
755.86	14.325 (0.011)	14.373 (0.023)	14.195 (0.028)	J. Espinoza
757.82	14.569 (0.011)	14.385 (0.019)	14.377 (0.031)	J. Espinoza
760.81	15.574 (0.058)	14.659 (0.054)	...	D. Gonzalez
763.84	15.879 (0.025)	14.693 (0.026)	14.585 (0.037)	D. Gonzalez
766.83	16.034 (0.023)	14.702 (0.029)	14.679 (0.032)	J. Espinoza
769.84	16.085 (0.052)	...	14.546 (0.045)	J. Espinoza
772.74	15.861 (0.028)	14.550 (0.020)	14.638 (0.038)	D. Gonzalez
775.77	15.486 (0.015)	14.425 (0.016)	14.402 (0.032)	D. Gonzalez
781.78	15.470 (0.018)	14.660 (0.017)	14.673 (0.029)	J. Espinoza
784.77	15.712 (0.018)	14.896 (0.020)	14.997 (0.040)	J. Espinoza
787.76	16.028 (0.037)	15.136 (0.044)	15.034 (0.083)	D. Gonzalez
791.74	16.376 (0.029)	15.261 (0.027)	15.662 (0.119)	D. Gonzalez
802.73	17.408 (0.094)	D. Gonzalez
812.84	...	16.519 (0.091)	...	J. Espinoza

Table 8. *JHK* Photometry of SN 2000cx. APO Data

JD+2451000	<i>J</i>	<i>H</i>	<i>K</i>	Observers
760.94	...	14.484 (0.025)	14.410 (0.110)	Krisciunas/McMillan
771.78	15.736 (0.047)	14.541 (0.023)	14.398 (0.033)	Krisciunas/Hastings/McMillan
777.88	15.153 (0.054)	14.452 (0.022)	14.606 (0.088)	Stubbs/McMillan/Hastings
778.76	15.136 (0.025)	14.483 (0.023)	14.500 (0.048)	Krisciunas/McMillan/Hastings
784.73	15.533 (0.037)	14.947 (0.027)	14.867 (0.064)	Rest/McMillan
788.77	15.909 (0.024)	15.287 (0.022)	15.326 (0.036)	Rest/Miknaitis/Hastings
834.76	18.149 (0.134)	17.910 (0.243)	...	Krisciunas/Bergeron

Table 9. Corrections from APO to YALO for *JHK* bands^a

JD+2451000	ΔJ	ΔH	ΔK
760.94	...	0.040	0.005
771.78	0.123	0.056	0.015
777.88	0.096	0.056	0.000
778.76	0.088	0.053	−0.001
784.73	0.117	0.011	0.002
788.77	0.153	−0.021	0.004

^aThese values are to be *added* to the APO data.

Table 10. Maximum Magnitudes of SN 2000cx

Filter	JD+2451000	m_{max}
<i>U</i>	751.9 (1.5)	13.19 (0.02)
<i>B</i>	752.5 (0.5)	13.42 (0.02)
<i>V</i>	753.7 (1.1)	13.25 (0.03)
<i>R</i>	753.5 (1.1)	13.34 (0.04)
<i>I</i>	750.2 (1.0)	13.65 (0.04)
<i>J</i>	749.9 (0.3)	13.85 (0.10)
<i>H</i>	749.0 (0.7)	14.04 (0.06)
<i>K</i>	749.5 (0.2)	13.98 (0.04)

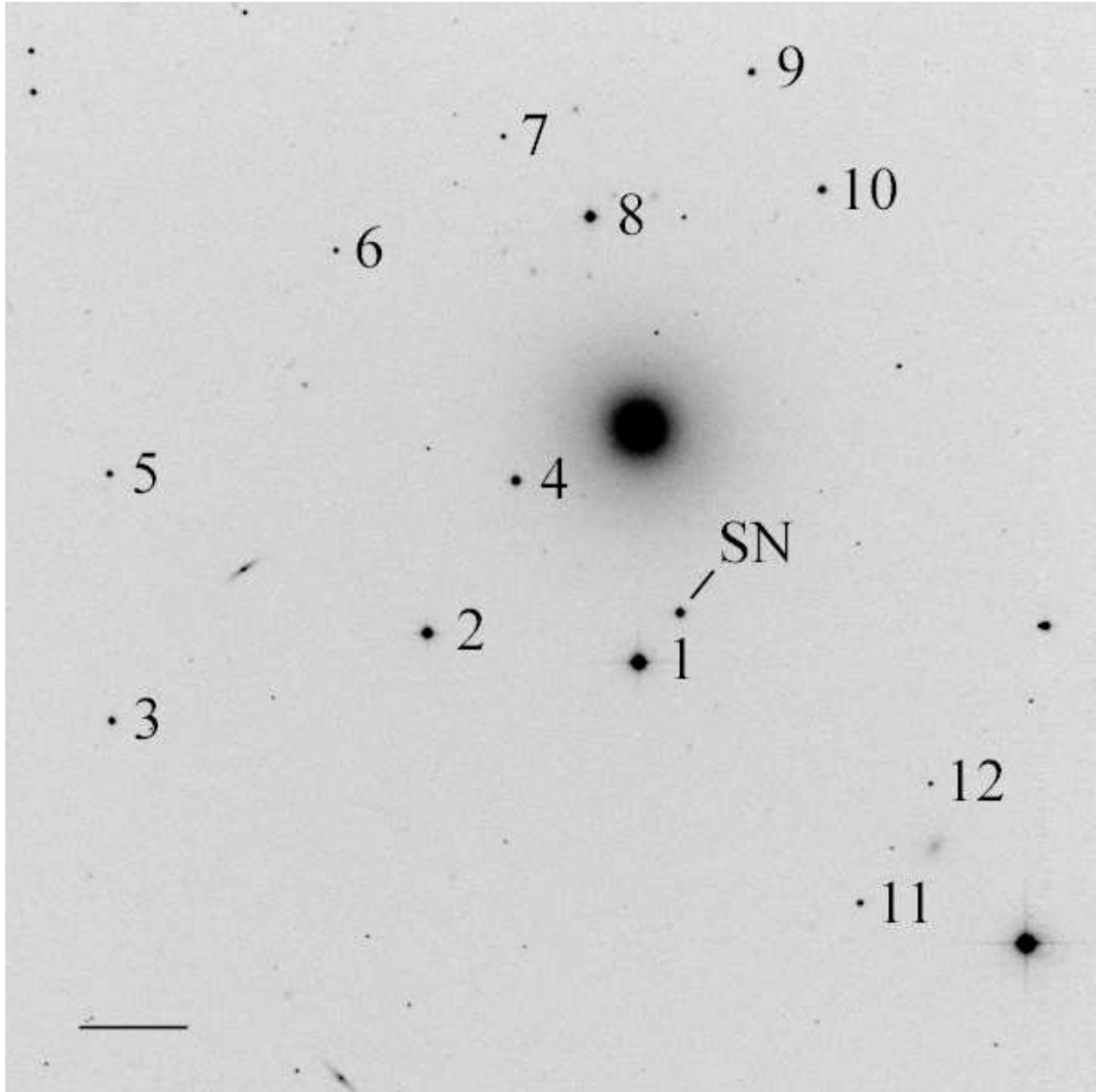


Fig. 1.— Finding Chart for local standards near SN 2000cx in NGC 524. The image is a combined *BVR* image taken with the CTIO 0.9-m telescope. N is up and E is to the left. The horizontal bar shows a scale of 1 arcminute.

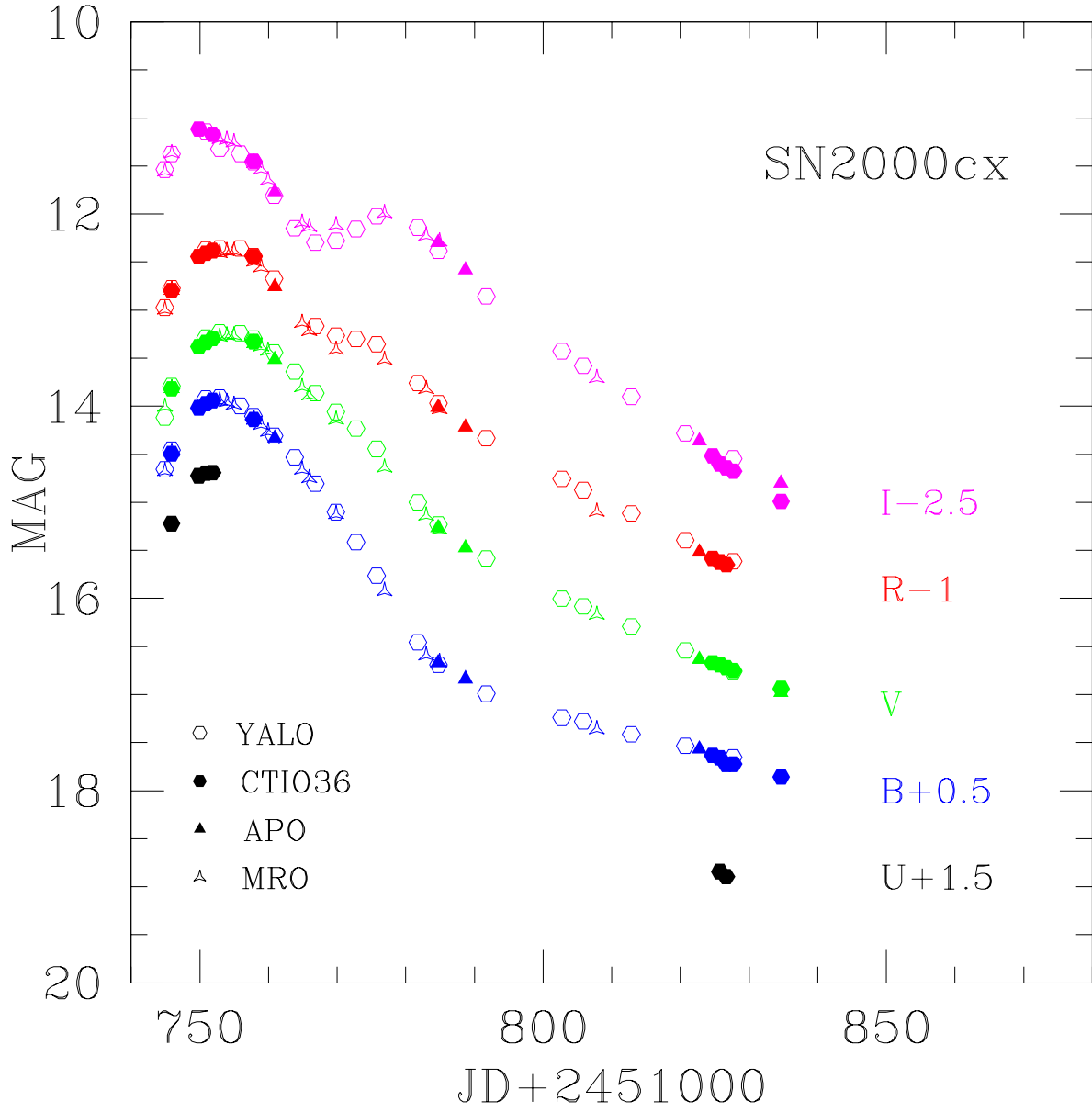


Fig. 2.— *U*-, *B*-, *V*-, *R*-, and *I*-band light curves of SN 2000cx, showing the optical data presented in this paper. The data are coded by telescope.

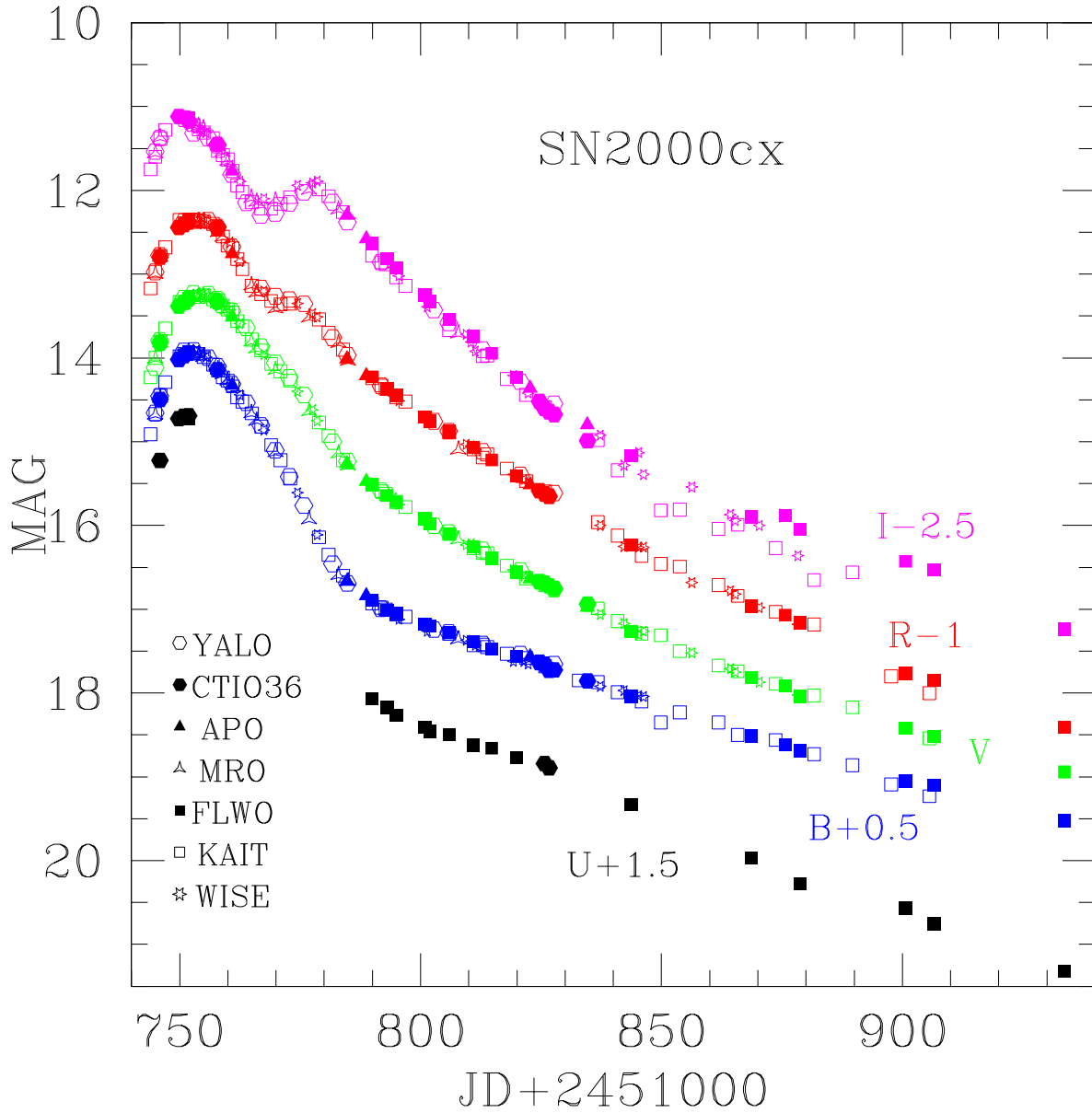


Fig. 3.— Same as Fig. 2, but with the addition of KAIT and Wise Observatory data given by Li et al. (2001), plus the Jha (2000) data obtained at the Fred L. Whipple Observatory.

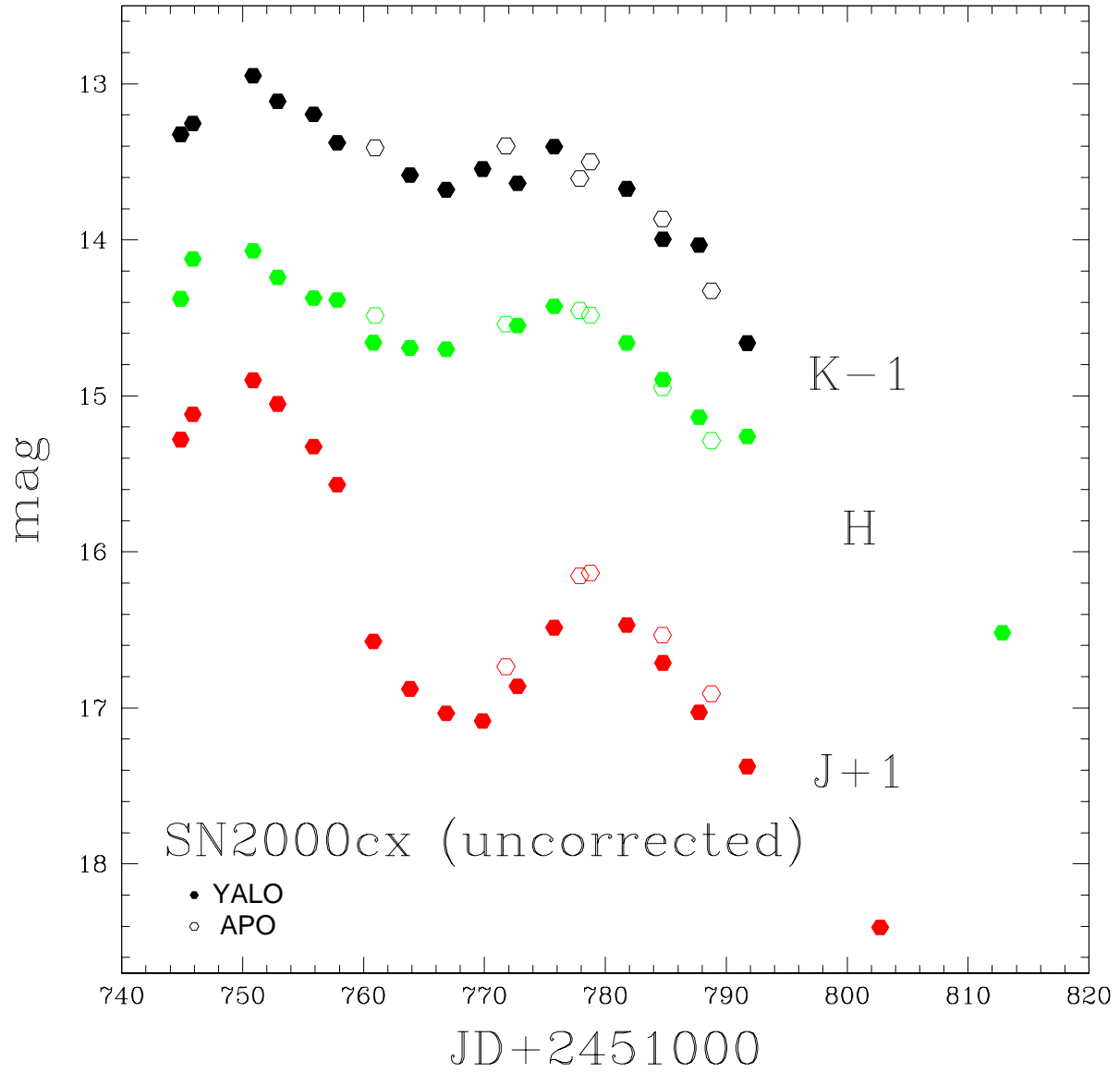


Fig. 4.— Infrared light curves for YALO and APO. The K - and J -band data have been offset by -1 and $+1$ magnitudes, respectively. APO data for Julian Date 2,451,834 are off the right hand side of the plot.

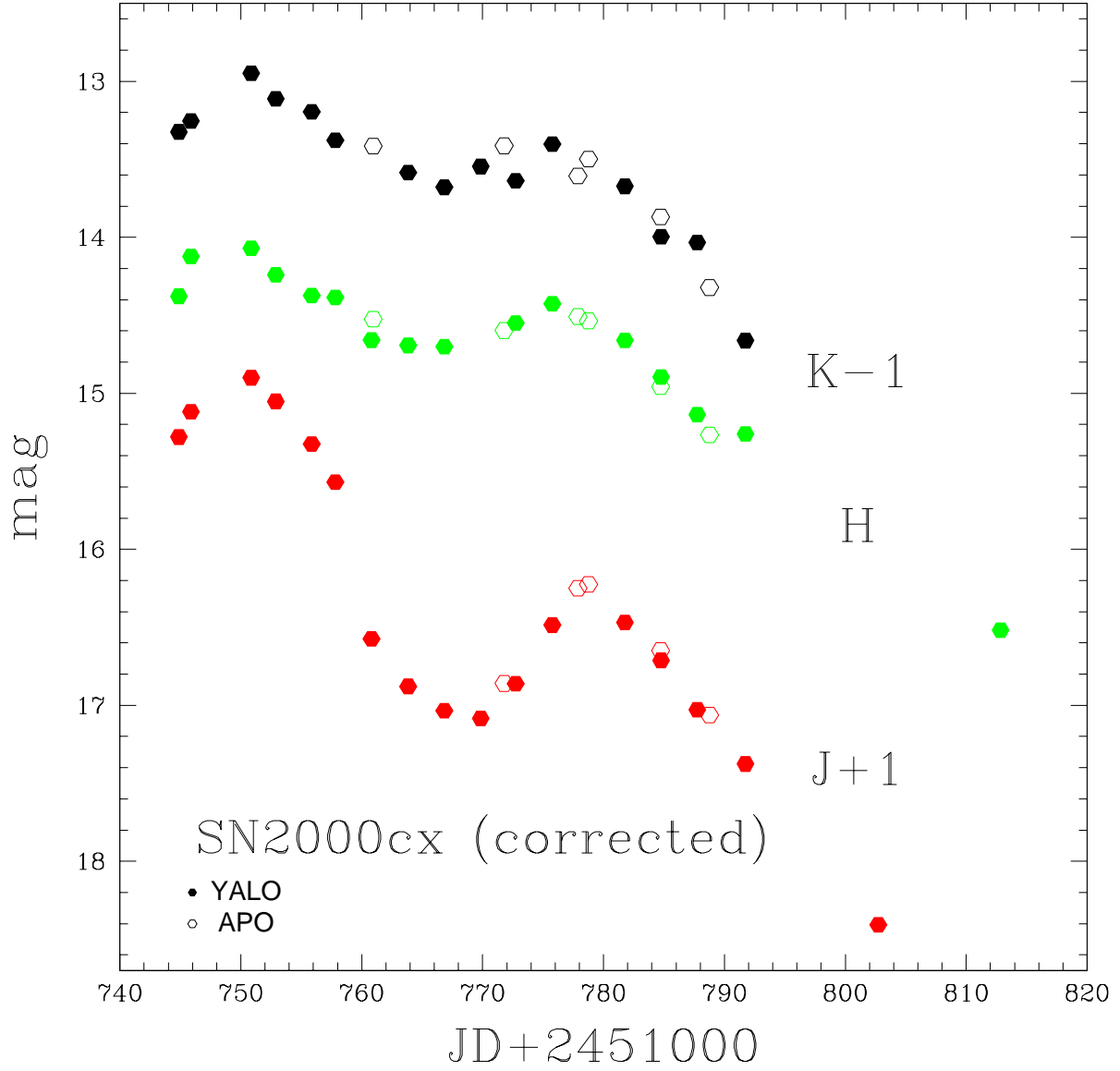


Fig. 5.— Same as Fig. 4, but the APO data have been corrected by the values given in Table 9.

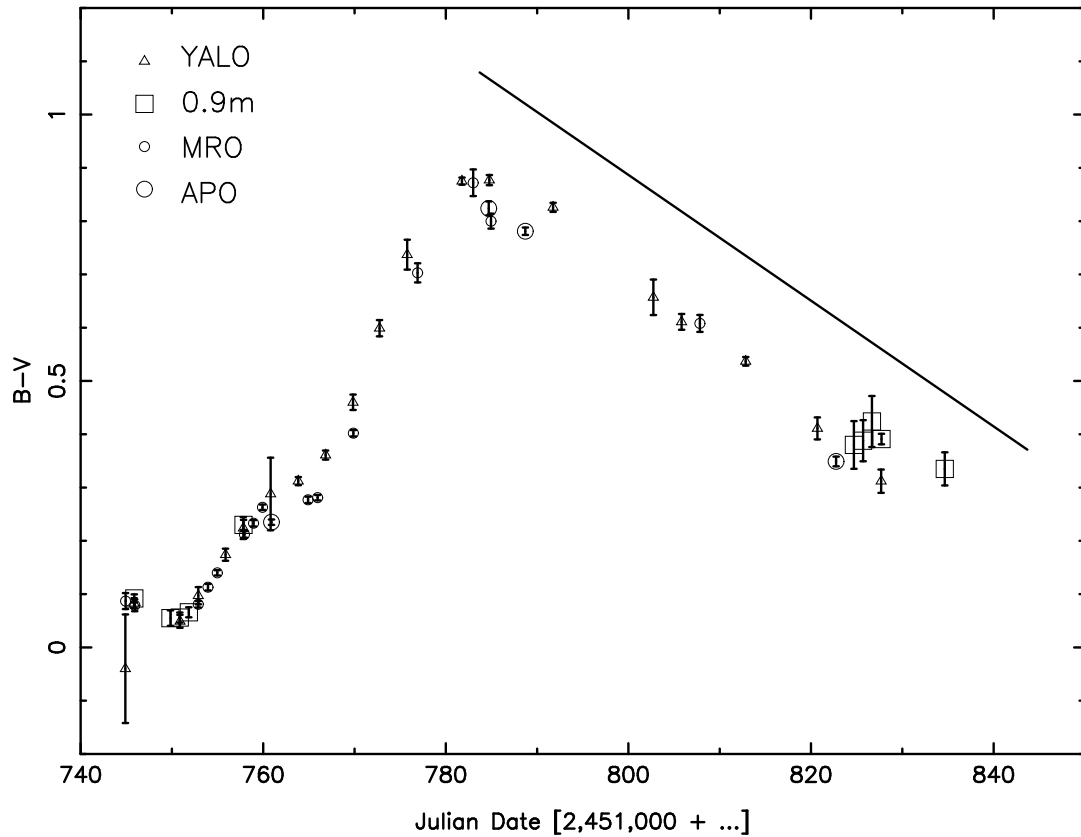


Fig. 6.— $B - V$ color curve of SN 2000cx, showing the optical data presented in this paper. $E(B - V) = 0.082$ has been subtracted from the data to eliminate the effect of dust in our Galaxy (Schlegel et al. 1998). The “zero reddening line” of Lira (1995) is shown, adjusted to the time of V -band maximum given in Table 10. If SN 2000cx has any host reddening, then the data points corresponding to unreddened photometry would be even further below the Lira line.

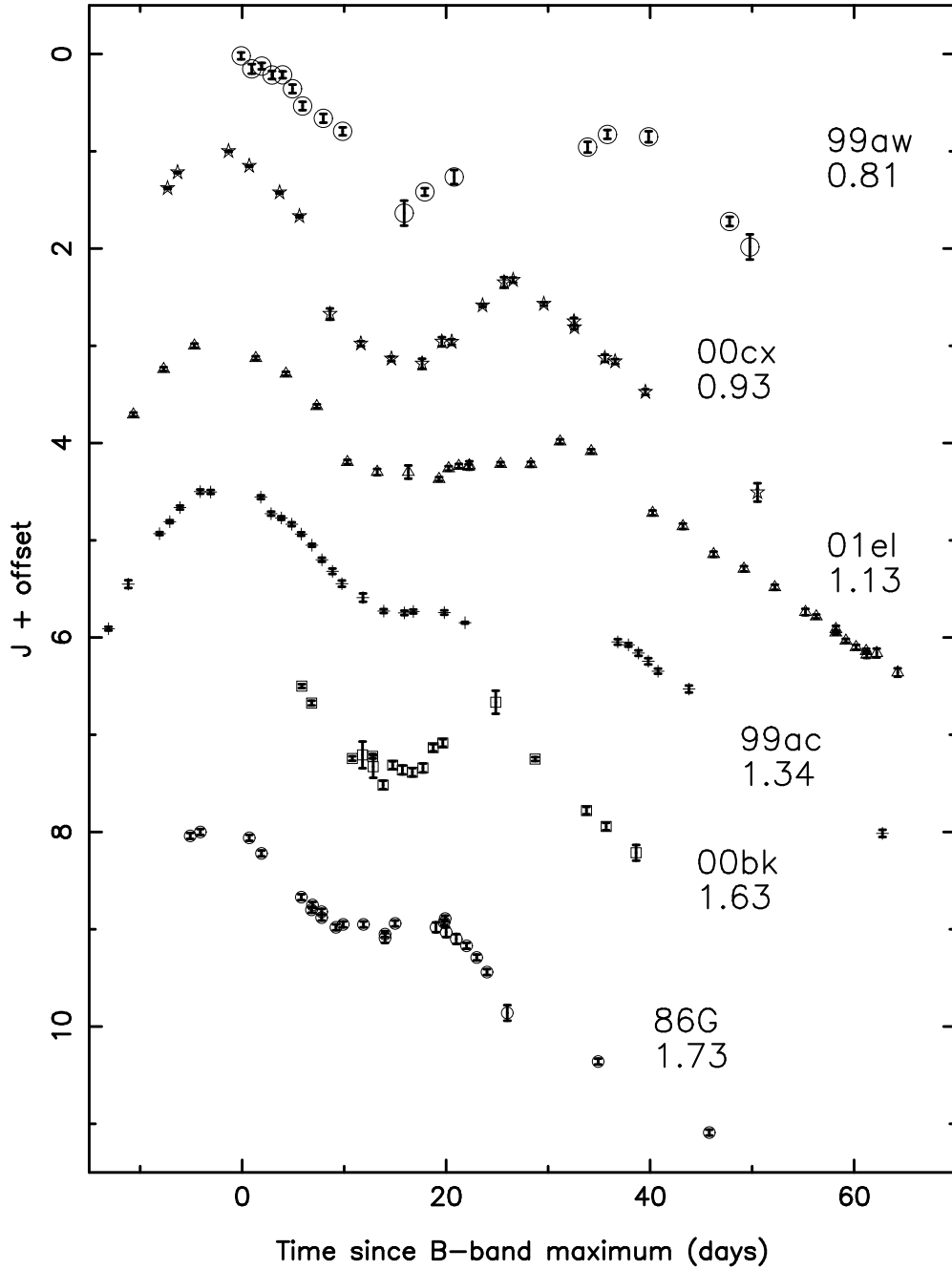


Fig. 7.— J -band light curve of SN 2000cx along with data of SNe 1999aw (Strolger et al. 2002), 2001el (Krisciunas et al. 2003), 1999ac (Phillips et al. 2002a, 2002b), 2000bk (Krisciunas et al. 2001), and 1986G (Frogel et al. 1987). The light curves are ordered from top to bottom by the decline rate parameter $\Delta m_{15}(B)$.

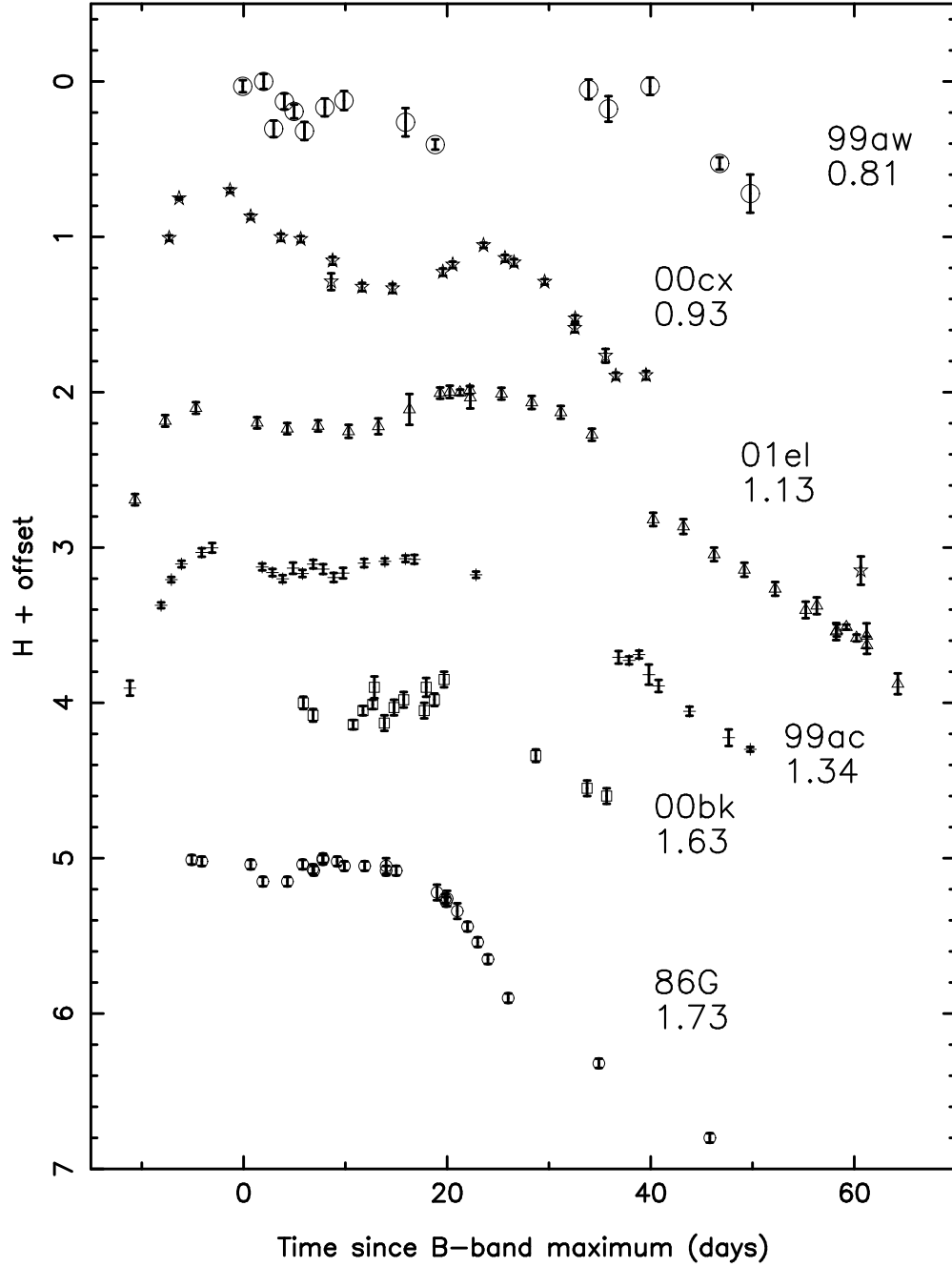


Fig. 8.— Same as for Fig. 7, but for the *H*-band.

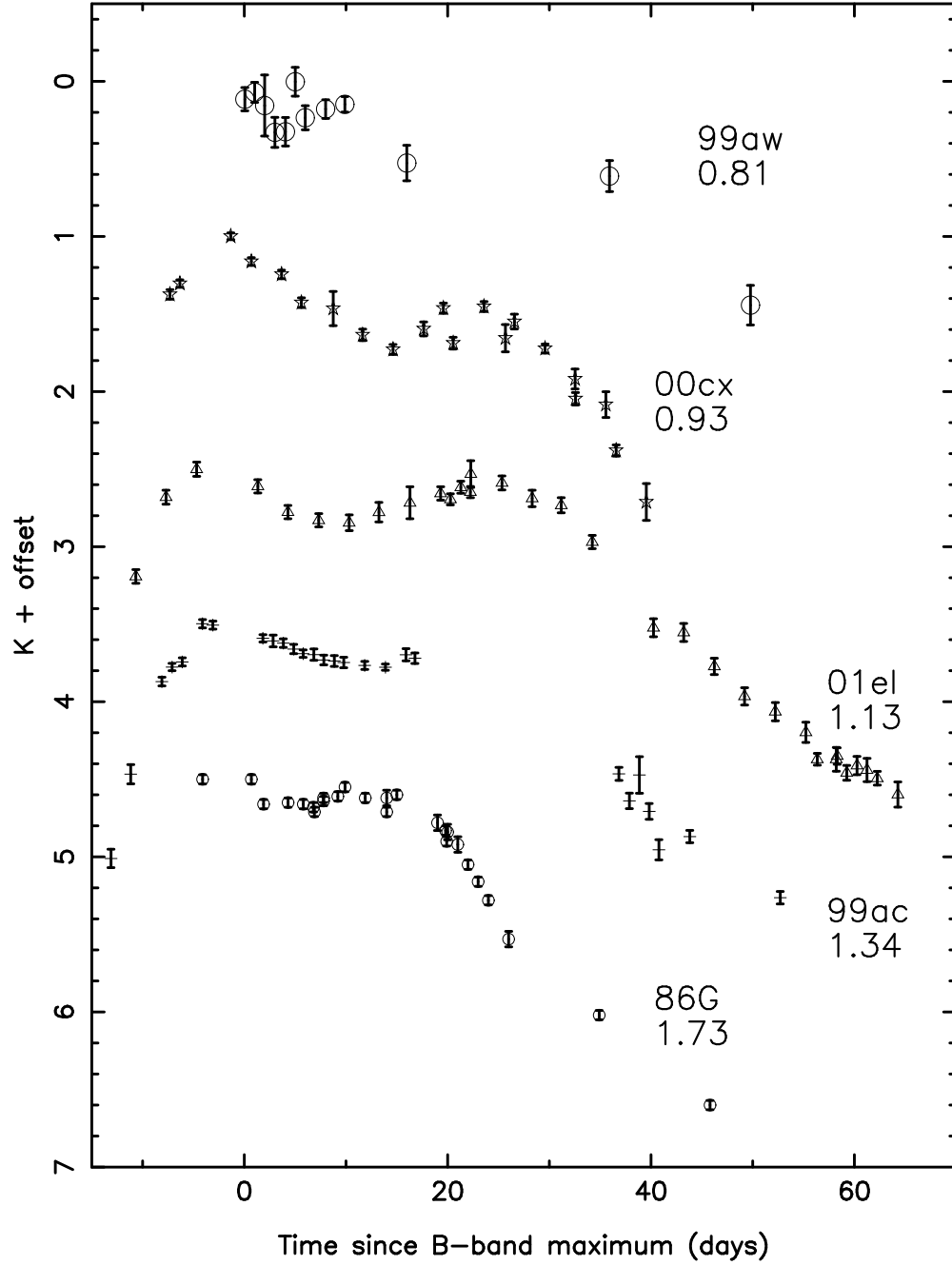


Fig. 9.— Same as for Fig. 7, but for the K -band. No K -band data were taken of SN 2000bk.

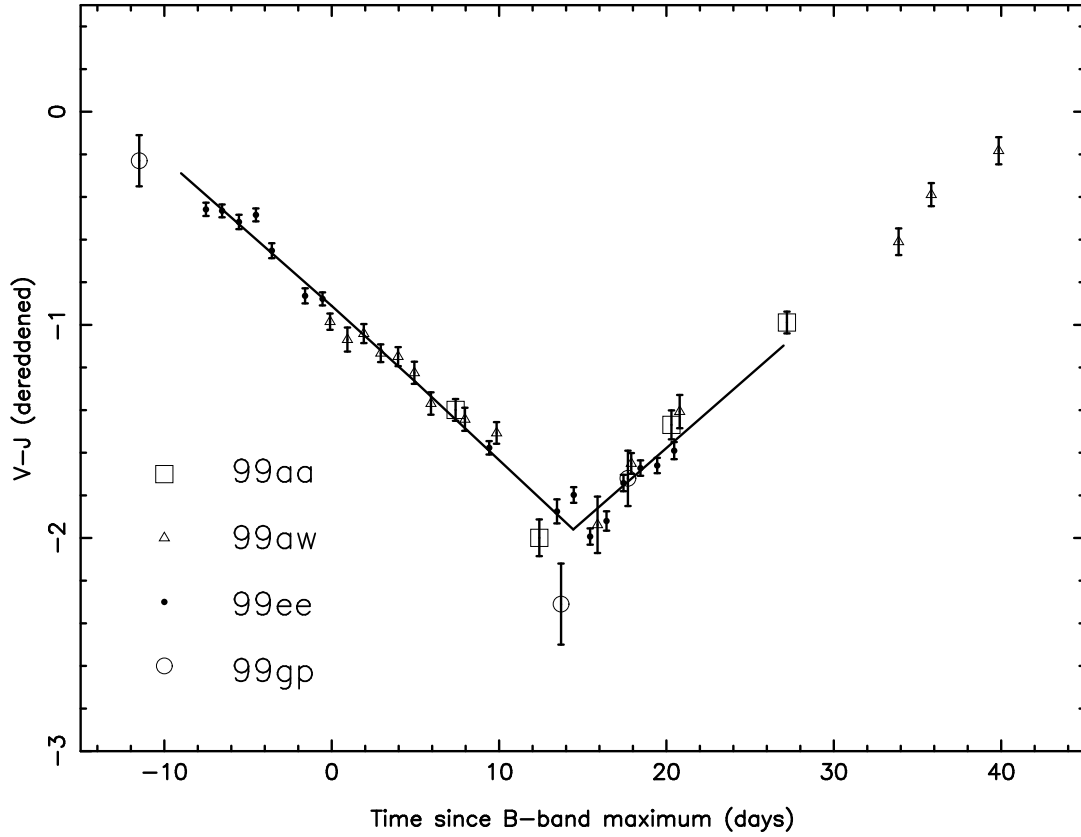


Fig. 10.— Dereddened $V - J$ colors of slowly declining Type Ia SNe. SNe 1999aa, 1999aw, and 1999gp were assumed to be unreddened in their host galaxies. For these three objects, only the reddening due to dust in our Galaxy has been subtracted (Schlegel et al. 1998). SN 1999ee has non-zero host reddening, which, along with its Galactic reddening, has been subtracted for the purposes of this graph.

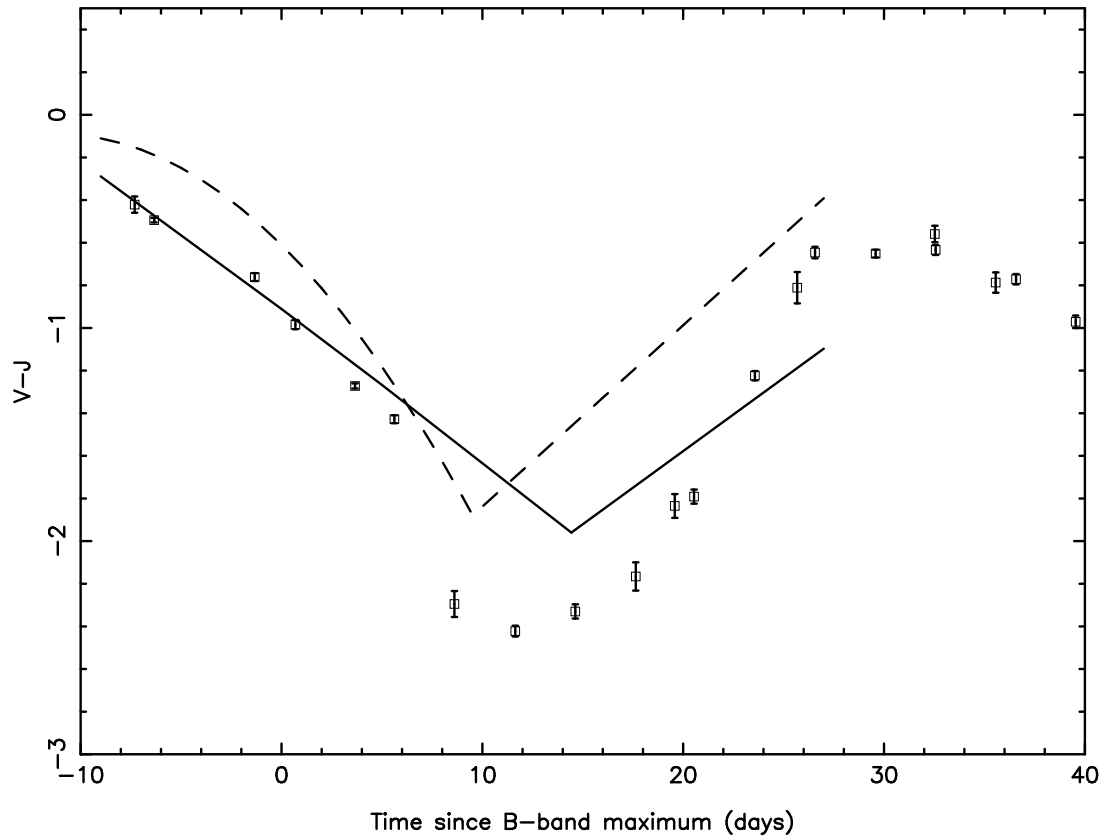


Fig. 11.— $V - J$ colors of SN 2000cx, with $E(V - J) = 0.182$ subtracted to account for the effect of dust in our Galaxy. The dashed line is the unreddened locus given by Krisciunas et al. (2000) for Type Ia SNe with mid-range B -band decline rates. The solid line is the unreddened locus derived from photometry of four slow decliners (SNe 1999aa, 1999aw, 1999gp, and 1999ee) shown in Fig. 10.

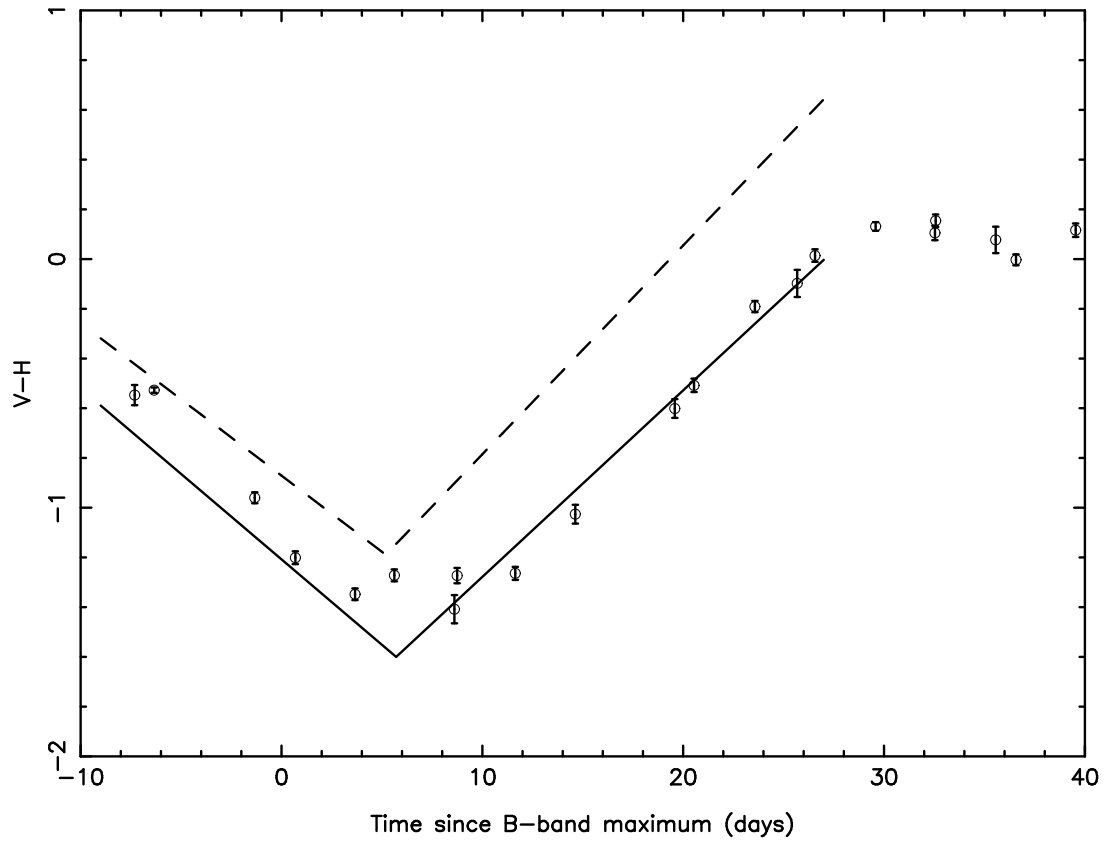


Fig. 12.— $V - H$ colors of SN 2000cx. The solid line is based on data of the slowly declining SNe 1999aw, 1999gp, and 1999ee. The dashed line is based on Type Ia SNe with mid-range B -band decline rates (Krisciunas et al. 2000). To eliminate the effect of dust in our Galaxy on the colors, $E(V - H) = 0.210$ mag has been subtracted from the SN 2000cx data.

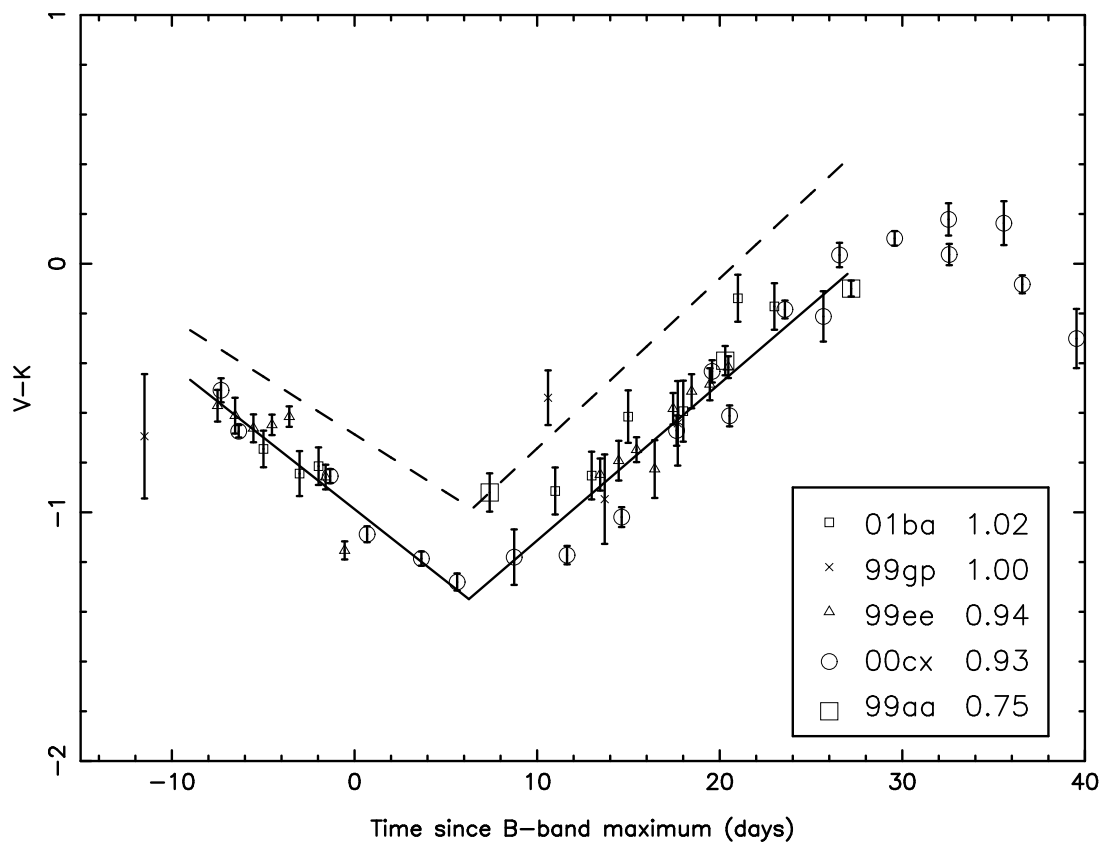


Fig. 13.— $V - K$ colors of SN 2000cx and four other slowly declining Type Ia SNe. The values of $\Delta m_{15}(B)$ are given in the box. The data of SNe 2000cx, 1999gp, and 1999aa have only been corrected for Galactic reddening (Schlegel et al. 1998). Data of SNe 1999ee and 2001ba have been corrected for host reddening and Galactic reddening. The dashed line is based on dereddened Type Ia SNe with mid-range B -band decline rates (Krisciunas et al. 2000). Clearly, the dereddened $V - K$ colors of the objects shown here are bluer than the locus based on mid-range decliners. From $10 < t < 21$ d the SN 2000cx data are the bluest.

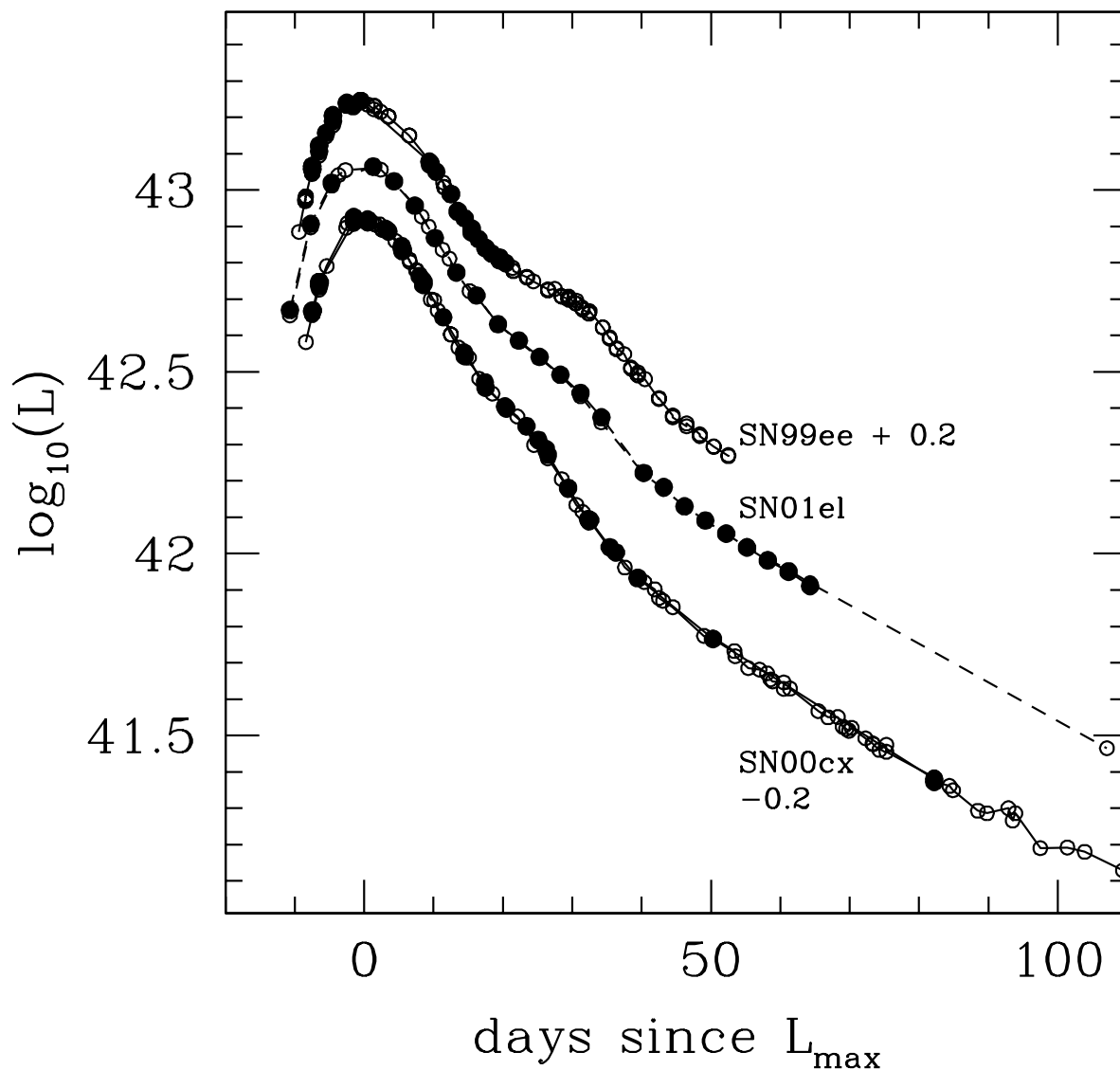


Fig. 14.— ”Uvoir” bolometric light curves for SNe 1999ee, 2001el, and 2000cx plotted against the time from maximum bolometric luminosity. The light curves for SN 1999ee and SN 2000cx have been shifted by +0.2dex (99ee) and –0.2dex (00cx) for clarity. We have assumed a distance modulus of 32.47 for SN 2000cx. The closed circles are the *UBVRIJHK* integrations and the open circles are the *UBVRI* integration. Both integrations include extrapolations to account for the missing flux outside of the integration limits. SN 1999ee and SN 2001el are normal Type Ia SNe with $\Delta_{m_{15}(B)}$ values of 0.94 and 1.13. Note the greatly reduced luminosity in the inflection point around day 30.

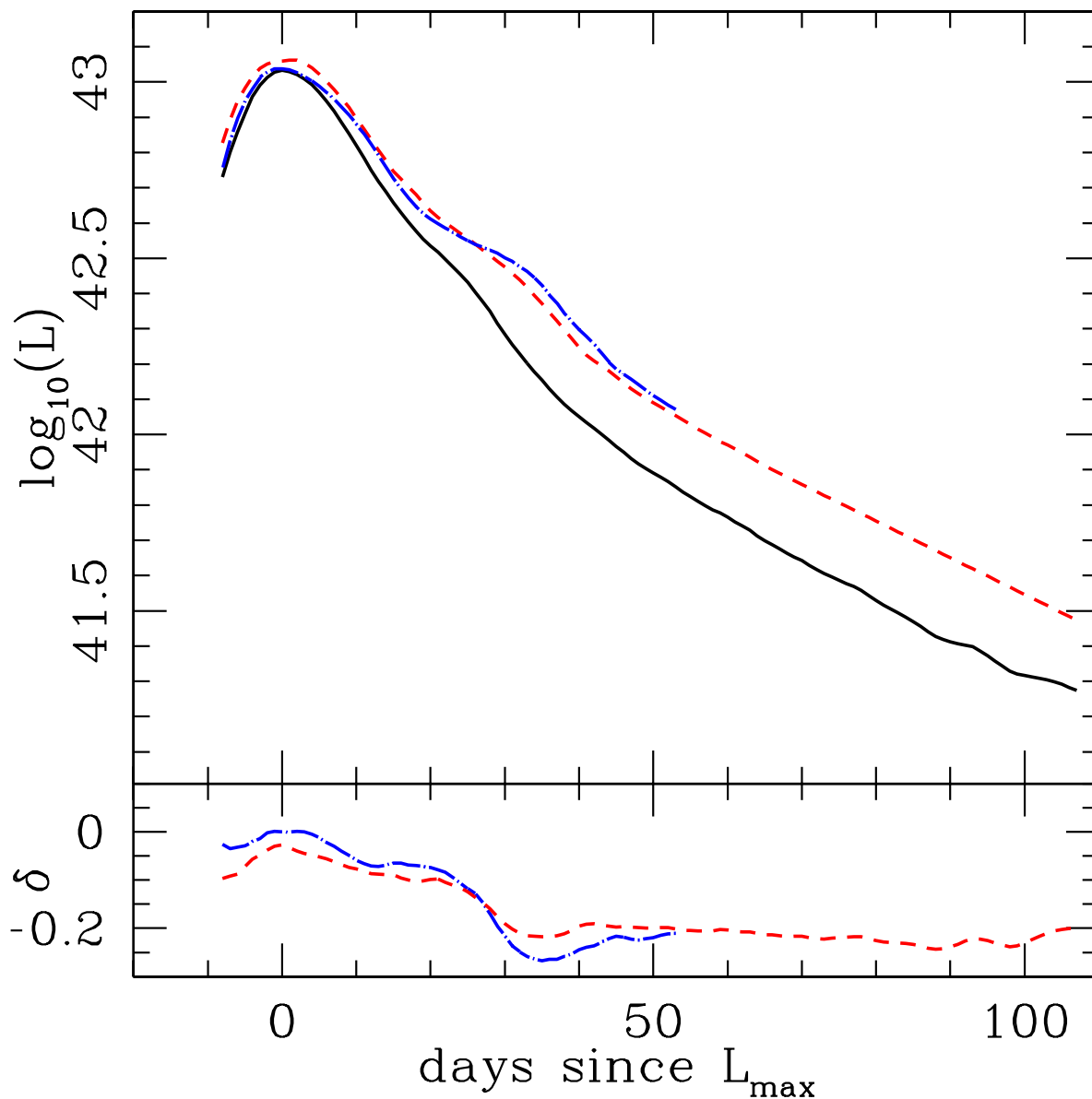


Fig. 15.— Smoothed curve representations of the “uvoir” bolometric luminosity for SN 2000cx (solid curve), SN 1999ee (dot-dashed curve), and SN 2001el (dashed curve). Note that the curves have not been shifted as they were in Fig. 14. The bottom panel shows the difference between the SN 2000cx bolometric light curve and the light curves for SN 1999ee (dot-dashed curve) and SN 2001el (dashed curve). This plot shows there are two major differences between SN 2000cx and these other “normal” Type Ia’s: the lack of bolometric flux around the time of the secondary I maximum at 30 days, and the low bolometric flux on the exponential tail after day 50 compared to the peak luminosity.

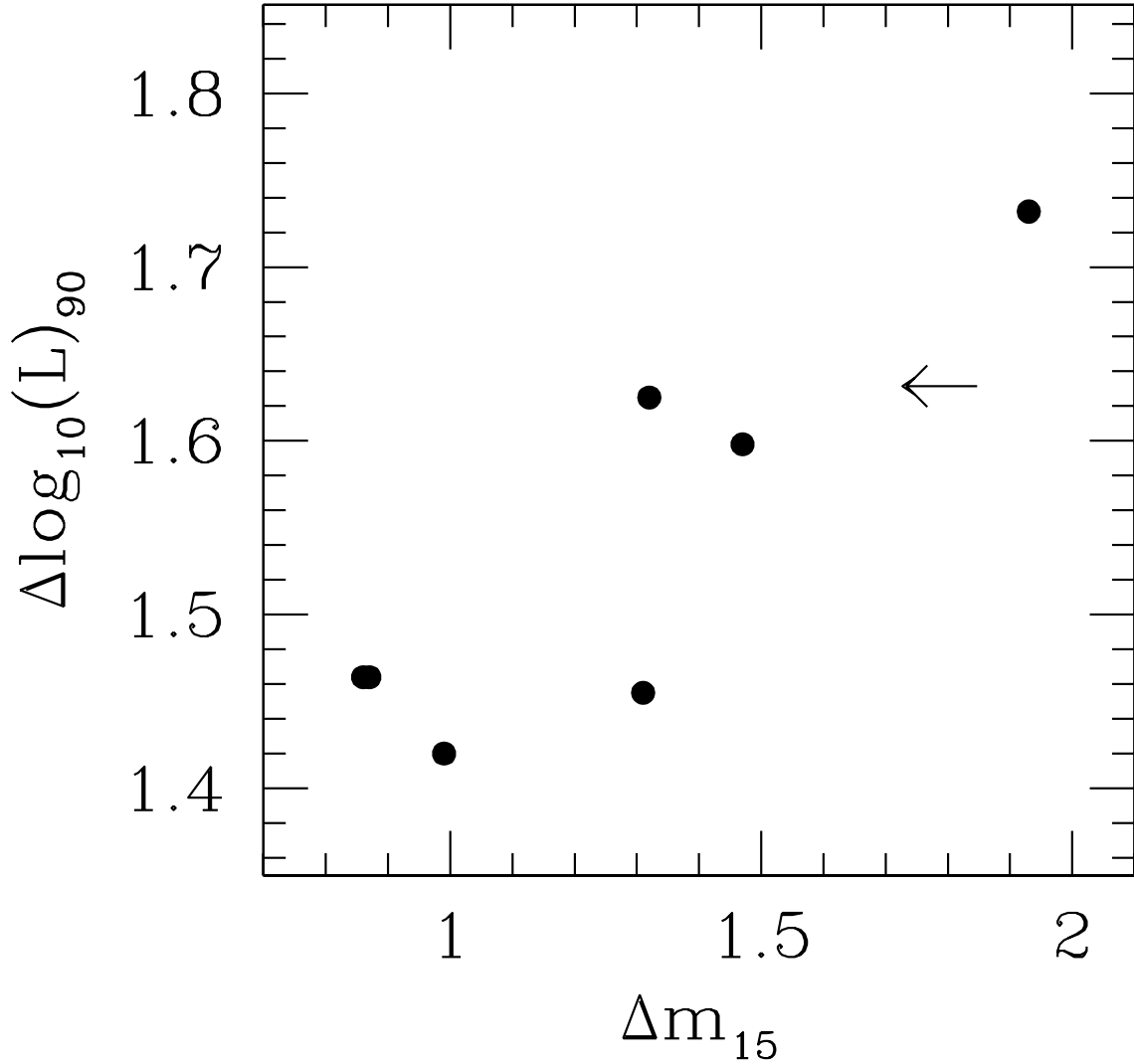


Fig. 16.— The difference in the peak bolometric luminosity compared to the luminosity 90 days after maximum light (in units of dex) for the sample of supernovae in Figure 5 of Contardo et al. (2000) as a function of $\Delta m_{15}(B)$. We mark the luminosity difference observed for SN 2000cx with an arrow. Evidently intrinsically fainter supernovae (those with larger Δm_{15}) have larger peak-to-tail luminosities. The position of SN 2000cx would associate it with the sub-luminous class of SNe.

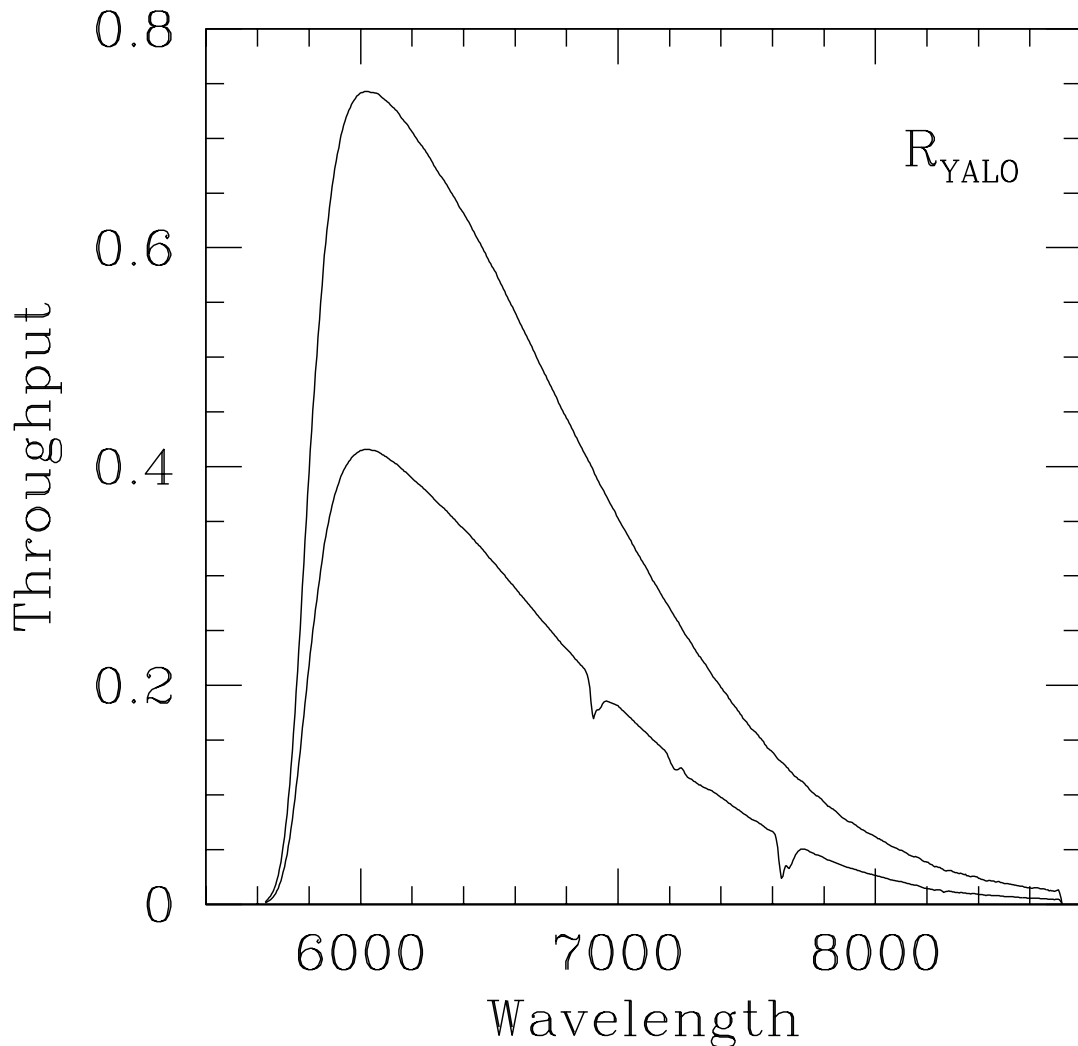


Fig. 17.— Upper curve: the transmission function of the R filter used for the YALO observations reported here. Lower curve: the filter transmission function multiplied by an atmospheric transmission function, quantum efficiency vs. wavelength, and two aluminum reflections, giving the effective transmission with the system for R . Both curves have been shifted 280 \AA to shorter wavelengths to account for the cooling of the filter in the dewar and so that the color term obtained from synthetic photometry matches that determined from observations of Landolt (1992) standards.